Development of PVDF-HFP Silica Superomniphobic Membrane for CO$_2$ Capture in Membrane Gas Absorption

by

Amanda Yap Yi Tong

18001492

Dissertation submitted in partial fulfilment of

the requirements for the

Bachelor of Engineering (Hons)

(Chemical Engineering)

JANUARY 2023

Universiti Teknologi PETRONAS,

32610, Bandar Seri Iskandar,

Perak Darul Ridzuan

CERTIFICATION OF APPROVAL

Development of PVDF-HFP Silica Superomniphobic Membrane for CO$_2$ Capture in Membrane Gas Absorption

by

Amanda Yap Yi Tong
18001492

A project dissertation submitted to the

Chemical Engineering Programme

Universiti Teknologi PETRONAS

in partial fulfilment of the requirement for the

BACHELOR OF ENGINEERING (Hons)

(CHEMICAL ENGINEERING)

Approved by,

_____

(AP Dr. Oh Pei Ching)

UNIVERSITI TEKNOLOGI PETRONAS

BANDAR SERI ISKANDAR, PERAK

January 2023

CERTIFICATION OF ORIGINALITY

This is to certify that I am responsible for the work submitted in this project, that the original work is my own except as specified in the references and acknowledgements, and that the original work contained herein have not been undertaken or done by unspecified sources or persons.

_____

AMANDA YAP YI TONG

ABSTRACT

In order to remove CO_2 from raw natural gas, membrane serves as a non-selective barrier between the acidic gas and the liquid absorbent in membrane gas absorption (MGA). However, the traditional hydrophobic membrane experiences problems such as pore wetting and long-term stability, which have a significant impact on membrane performance. This has prompted the improvement of membrane hydrophobicity toward a superomniphobicity surface in order to reduce the tendency of wetting and increase CO_2 absorption flux in MGA systems. In this research, PVDF-HFP superomniphobic membrane is developed by incorporating different silica nanoparticles and chemical additives to evaluate its effect on membrane superomniphobicity. 0.06 wt% LUDOX HS-40 colloidal silica nanoparticles and 0.06 wt% NH_2 functionalized silica nanoparticles are incorporated as non-solvent additives to investigate the order of silica nanoparticles addition on membrane superomniphobicity. The long-term operational stability of membranes for MGA system is assessed by exposing the membranes to liquid absorbent for 0, 3 and 6 days. By immersing in FAS/n-Hexane bath, M-H membrane exhibited higher water and MDEA contact angles compared to the pristine membrane. Further enhancement of membrane superomniphobicity was done by incorporating 0.06 wt% LUDOX HS-40 colloidal silica nanoparticles as non-solvent additive in ethanol coagulation bath, which denoted as M-L2. M-L2 membrane achieved superomniphobicity with water contact angle of $164.97 \pm 2.81^{\circ}$ and MDEA contact angle of $153.31 \pm 2.13^{\circ}$. The incorporation of non-solvent additive was found to be more effective in improving membrane superomniphobicity in term of contact angle and porosity. Upon immersion, M-L2 membrane exhibited the highest CO_2 absorption flux and operational stability due to its higher wetting resistance. In comparison to a pristine membrane, the M-L2 membrane in the MGA system showed 1.95 times greater operational stability. Further research on hollow fibre superomniphobic membrane could be done.

ACKNOWLEDGEMENTS

First, I would like to express my deepest gratitude to my supervisor, AP Dr. Oh Pei Ching, for her knowledge and patience, which have been a great source of encouragement and inspiration throughout the journey of Final Year Project. In addition, her professional experiences and constant guidance from the beginning to the end of the Final Year Project assist me in gaining a better comprehension of the field of study investigated. In addition, the fact that she read my work with diligence and perseverance contributed to my desire to pursue excellence.

In addition, I would like to extend my gratitude to Universiti Teknologi PETRONAS (UTP) Malaysia for providing me with support to complete Final Year Project. My gratitude also extends to the members and staffs of the Chemical Engineering Department, CO_2 Research Centre (CO2RES) and Centralized Analytical Laboratory (CAL) for providing equipment training, lab inductions and technical support. I would like to acknowledge MTDC Lab, School of Chemical Engineering, Universiti Sains Malaysia (USM) for their assistance with the experiments conducted.

My family, particularly my parents, deserve many thanks for raising me and always being there for me. The journey towards completing this dissertation would not be possible without the assistance of my parents and siblings. Lastly, I would like to extend my regards to my friends, who have provided me with sufficient moral support, technical advice and confid

TABLE OF CONTENTS

LIST OF FIGURES

LIST OF TABLES

LIST OF ABBREVIATIONS

AFM	Atomic Force Microscopy
APTES	3-Aminopropyl Triethoxysilane
CA	Contact Angles
CB	Cassie-Baxter
CF_2	Difluorocarbene
CF_3	Trifluoromethyl Radical
CH_2	Methylene
CH_3	Methyl Radical
CO_2	Carbon Dioxide
DCMD	Direct Contact Membrane Distillation
DI	Deionised
DMAC	N-Dimethylacetamide
EDX	Energy Dispersive X-Ray Spectroscopy
FAS	1h,1h,2h,2h-Perfluorooctyltriethoxysilane
FluoroPOSS	Fluorinated Polyhedral Oligomeric Silsesquioxanes
F-POSS	Heptadecafluorodecyl Polyhedral Oligomeric
LEP	Liquid Entry Pressure
MDEA	N-methyldiethanolamine
MEA	Monoethanolamine
MGA	Membrane Gas Absorption
NaOH	Sodium Hydroxide
NIPS	Non-Solvent Induced Phase Inversion Technique
NMP	N-Methyl-2-Pyrrolidone
OCA	Optical Contact Angle
PDMS	Polydimethyl Siloxane
PE	Polyethylene
PORPLUX	Capillary Flow Porometer
PP	Polypropylene
PSA	Pressure Swing Adsorption
PTFE	Polytetrafluoroethylene
PVDF	Polyvinylidene Fluoride

PVDF-HFP	Poly (Vinylidene Fluoride-Co-Hexafluoropropylene)
RA	Rolling-Off Angles
RH	Relative Humidity
SEM	Scanning Electron Microscopy
SiNP	Silica Nanoparticles
SOM	Superomniphobic Membrane
VIPS	Vapor-Induced Phase Separation Technique

CHAPTER 1

INTRODUCTION

1.1   Background

Raw natural gas is one of the most important fuel sources worldwide (Baker, 2021). The demand for natural gas demand reaches a peak in 2021 at 4,000 billion cubic meters compared to 2,900 billion cubic meters in 2005. According to International Energy Agency, it is predicted that global natural gas consumption would increase at an average annual rate of 0.8% from 2022 to 2025, reaching roughly 4,240 billion cubic meters (International Energy Agency, 2022). The raw natural gas that is extracted from wells contains a wide variety of contaminants, including carbon dioxide, hydrogen sulphide, nitrogen, water and other chemicals. They originate from crude oil wells, gas wells and condensate wells, which are the three distinct types of producing wells (Mokhatab et al., 2019). One of the sources of natural gas is extracted from wells located offshore. Unconventional sources often have a high concentration of CO_2. It is anticipated that these gas reserves are far greater than previously estimated. As exploration and drilling technology develops, unconventional deposits become economically viable and they will become a significant source of energy supply (Mokhatab et al., 2019).
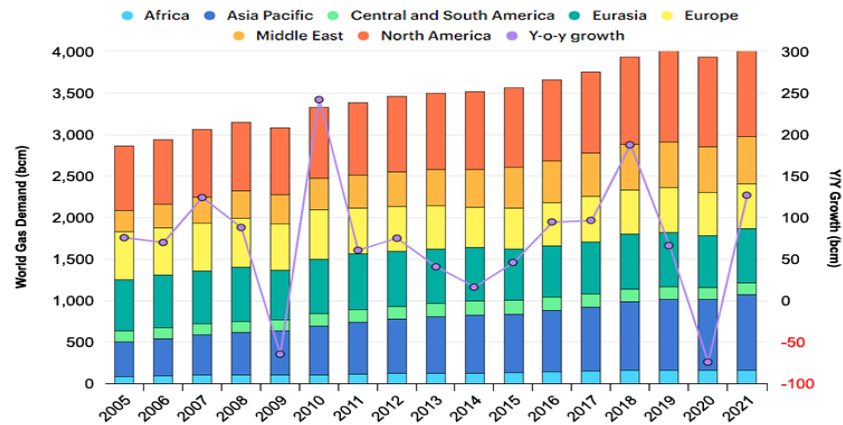
Figure 1.1: Evolution of natural gas demand from 2005 to 2021 (International Energy Agency, 2022)

According to Khan et al. (2018), it is found that the CO_2 content of natural gas fields in Malaysia and other Southeast Asia offshore fields ranges from 28% to 87%. In Malaysia, the Peninsular average CO_2 fraction is around 46% as shown in Figure 1.2. Whereas, at Sarawak, the average CO_2 fraction is higher than the average CO_2 fraction at Peninsular. It contains 72% CO_2 gas fraction and 28% hydrocarbon gas fraction (Darman & Harun, 2016). High concentrations of CO_2 in natural gas will lead to pipeline corrosion, increased compression costs and a drop in heating value, making its removal exceedingly difficult. Thus, it is important to capture and eliminate the presence of carbon dioxide (Buonomenna, 2017).
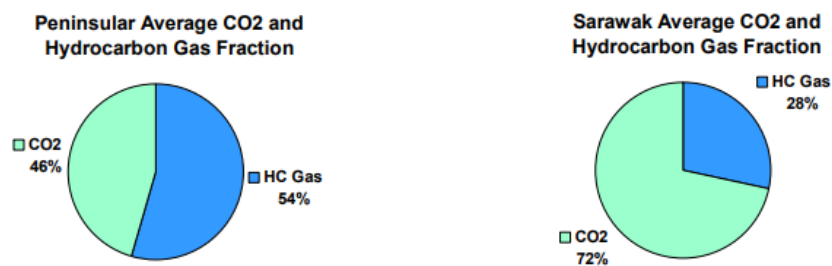
Figure 1.2: Average CO_2 and hydrocarbon gas fraction (Darman & Harun, 2016)

Conventionally, CO_2 capture has been performed by the gas absorption process in a variety of reactor types, including packed towers, venturi scrubbers, bubble columns and sieve trays. Despite the fact that traditionally packed bed absorbers have been used in the chemical industry for many decades, there are still a number of drawbacks

2

associated with the use of these types of absorbers. (Ahmad et al., 2010). There are some issues that arise when transferring carbon dioxide from the gaseous to the liquid phase, including flooding at high flow rates, unloading at low flow rates, channelling and foaming.

Recently, a nondispersive contactor through a microporous membrane, also known as membrane gas absorption (MGA), has emerged as a viable alternative technique for capturing CO_2 that not only addresses these drawbacks but also provides greater interfacial area than the traditional methods. Membrane gas absorption (MGA) provides an efficient method for capturing CO_2 at a low cost and pressure. In membrane gas absorption (MGA), the contactors that are employed for the effective uptake of CO_2 into liquid absorbent are typically microporous membranes (Ahmad & Ramli, 2013). Although the particular gas–liquid interfacial area in MGA is rather large, it is important to avoid membrane wetness in order to keep the barrier to mass transfer in the pores to a minimum. The material of the membrane has to be hydrophobic in order to limit the wetting that occurs in the pores. Some issues regarding the material of membrane must be addressed before this technology can be implemented on the industrial basis. Superomniphobic membrane, which is liquid-repellent membranes, has been introduced to capture carbon dioxide in order to overcome the limits of traditional membranes. Most common materials are polypropylene (PP), polyethylene (PE), polytetrafluoroethylene (PTFE) and polyvinylidene fluoride (PVDF) (Chiao et al., 2022).

1.2   Problem Statement

In the long-term run of MGA system, the traditional hydrophobic membrane might experience pore wetting. The term "pore wetting" refers to the phenomenon in which liquid, as opposed to vapour, is present inside the pores of a membrane (Chamani et al., 2021). Wetting the membrane pores drastically reduces membrane performance because gas diffusion is drastically hindered in the almost stationary liquid layer (Geyer et al., 2017).

Besides, the order of silica nanoparticles addition to membrane might be a problem as the incorrect order of silica nanoparticles addition affects membrane superomniphobicity, porosity and CO_2 mas transfer rate. Agglomeration of silica nanoparticles might happen due to the incorrect order of silica nanoparticles addition (Sabzekar et al., 2022). This phenomenon will result in the reduction of membrane porosity. Since the membrane's low porosity reduces the contact area between the gas and liquid phases, it increases the barrier to gas transport and slows the diffusion of CO_2 (Wang et al., 2022). The mass transfer rate across a membrane deteriorates with decreased porosity (Khan et al., 2018).

Additionally, the membrane's long-term stability when it is implemented in industry is a concern during carbon dioxide capture since most membrane materials have low mechanical stability, low thermal stability and inadequate chemical resistance to the alkaline capturing solution (Geyer, Schönecker, Butt, & Vollmer, 2016). As a result, the membrane phase's mass transfer stability and operational performance deteriorate significantly.

1.3 Objectives

Three major objectives have been identified for this research.

1. To evaluate the influence of silica nanoparticles and chemical additives on membrane superomniphobicity

2. To investigate the order of silica nanoparticles addition on membrane superomniphobicity

3. To assess the stability on the synthesized superomniphobic membrane for the membrane gas absorption (MGA) system

1.4 Scope of Study

The superomniphobicity of membranes, the synthesis, characterisation and CO_2 absorption performance evaluation are the primary focuses of this study. Consequently, in order to meet the objective of this research, the scope of the study is defined and described as follows.

Objective 1: Evaluation of Influence of Silica Nanoparticles and Chemical Additives on Membrane Superomniphobicity

The membrane is synthesized using poly (vinylidene fluoride-co-hexafluoropropylene) (PVDF-HFP) as the polymer and *N*-methyl-2-pyrrolidone (NMP) as the solvent. The techniques used are non-solvent induced phase inversion technique (NIPS) and vapor-induced phase separation technique (VIPS). The first layer is fabricated using NIPS to generate a tiny mean pore size and a regulated pore size distribution, while the second layer is fabricated using VIPS to create macro corrugations and accomplish the desired superomniphobicity and roughness. In order to achieve superomniphobicity, silica nanoparticles and chemical additives are added to investigate the influence on membrane superomniphobicity. Different chemical additives, which are 7.5 M NaOH aqueous solution, 3% v/v APTES/ethanol, net spacer and 1% v/ v FAS/n-Hexane, are used to investigate the influence on membrane superomniphobicity. Besides, 0.06 wt%

LUDOX HS-40 silica nanoparticles and 0.06 wt% NH_2 functionalized silica nanoparticles are utilized to examine the impact on membrane superomniphobicity.

Objective 2: Investigation of Order of Silica Nanoparticles Addition on Membrane Superomniphobicity

The order of silica nanoparticles addition on membrane superomniphobicity is investigated by incorporating 0.06 wt% LUDOX HS-40 colloidal silica nanoparticles and 0.06 wt% NH_2 functionalized silica nanoparticles after PVDF-HFP membrane is fabricated. The order is manipulated by incorporating 0.06 wt% LUDOX HS-40 colloidal silica nanoparticles and 0.06 wt% NH_2 functionalized silica nanoparticles as non-solvent additives, which indicates that the silica nanoparticles is added during the immersion of membrane in ethanol bath.

Objective 3: Evaluation of Operational Stability of Synthesized Membrane

Membrane gas absorption is used to determine the absorption performance of the synthesized membrane in terms of CO_2 absorption flux. Pure CO_2 gas is used as the feed gas and monoethanolamine (MEA) is used as the liquid absorbent during membrane testing. The long-term operational stability of membranes is evaluated by exposing the membrane surface to liquid absorbent for 0, 3 and 6 days.

CHAPTER 2

LITERATURE REVIEW

2.1 CO_2 Removal Technologies

In order to preserve the energy content and prevent damage to downstream units, it is necessary to capture CO_2 from natural gas. The high level of CO_2 will result in pipeline corrosion, compression costs and decrease in heating value (Buonomenna, 2017). Conventional strategies to capture CO_2 include chemical or physical absorption, cryogenic distillation, solid adsorption, membrane separation and membrane gas absorption as shown in Figure 2.1.
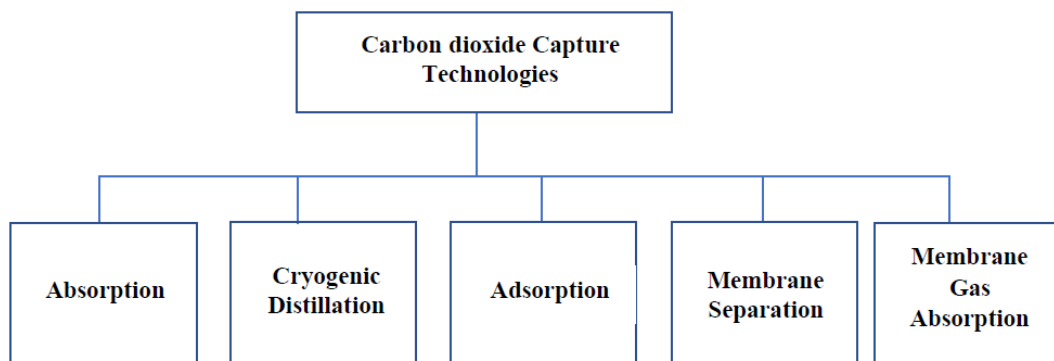
Figure 2.1: CO_2 capture technologies

2.1.1   Membrane Separation

The membrane of a gas-liquid membrane contactor separates the feed gas from the absorbing liquid. Factors such as the kinetic diameter or chemical interactions between the gas and material allow gas separation membranes to preferentially

penetrate certain gas molecules (Kim et al., 2021). CO_2 is separated from other gases by diffusing through the membrane and being absorbed by the selective absorption liquid, as shown in Figure 2.2. The liquid is circulated from the absorber to the desorber, where CO_2 is desorbed. The membrane might be non-selective and operate as a simple barrier, or it can be selective as in research targeted at avoiding wetting for high-pressure applications (Buonomenna, 2017). Since membrane-based separation does not need a phase change, it is efficient and requires a small amount of energy. However, it operates most efficiently with high partial pressure in the feed gas stream (Kim et al., 2021).
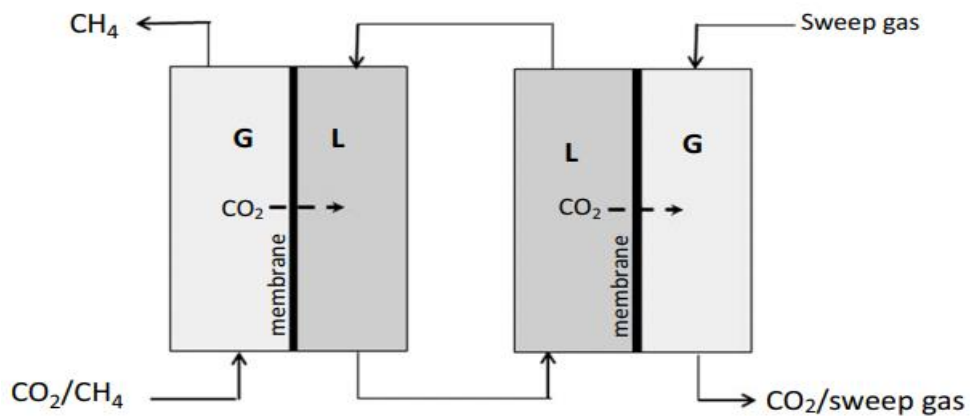
Figure 2.2: Schematization of a gas/liquid membrane contactor (Buonomenna, 2017)

2.1.2   Adsorption

A competitive capture mechanism that has been researched in the industry is adsorption on porous solid adsorbents employing pressure swing adsorption or temperature swing methods for the purpose of capturing CO_2 (Gopalan et al., 2022). The molecules of carbon dioxide will experience a drop in free energy as they get closer to the adsorbent's surface. The gas molecules will be attracted to the adsorbent surface's electrical environment in this situation. The amount of CO_2 molecules that are present at the adsorbent surface increases as a result of the interactions between the gas molecules and the solid surface, as well as the corresponding drop in entropy (Abd et al., 2020). As van der Waals forces are involved, adsorption could occur. In addition to this, it is possible for it to exist chemically, which would require the creation of a

chemical bond between the surface of the adsorbate and the adsorbent (Abd et al., 2020). Solid adsorbents for CO_2 removal have many advantages compared to other methods, such as high CO_2 uptake, high recovery and stability of materials, high effectiveness even in humid environment and lower overall cost (Hussin & Aroua, 2020).

2.1.3 Absorption

In the process of purifying natural gas, gas absorption is one of the most essential unit activities that may be performed. The process is often carried out in a vertical tower with counter-current, in which the gas mixture is brought into direct contact with liquid absorbent in order to selectively dissolve desired gas components. In a stripping column, the liquid absorbent is recovered by releasing CO_2 and reusing it for gas absorption. Large-scale industrial applications of carbon dioxide capture at the source rely mostly on chemical and physical absorption methods that use a wide range of solvents as absorbents (Arshadi et al., 2019). Water, methanol, polyethylene oxide and ethanol are examples of these solvents (Z. Zhang et al., 2018). The type of solvents is the most important factor to consider when evaluating the CO_2 absorption capacity.

2.1.4 Cryogenic Distillation

A physical process known as cryogenic separation is used to separate CO_2 which takes place at extremely low temperatures. Instead of compressing gaseous CO_2 to very high pressure, it is possible to directly create liquid CO_2 at low pressure, which can then be stored or sequestered via liquid pumping (Xu et al., 2014). This results in savings in compression energy. The components of gas mixtures are separated via a method known as cryogenic separation, which involves a number of phases that involve separation, refrigeration and compression of the components. The functioning of these processes, as well as the practicality of their design, can be assuredly ensured because the technologies involved in the chemical industry have reached a very mature

stage (Song et al., 2012). The cryogenic separation technique does not involve the use of any chemical agents, which eliminates the possibility of secondary contamination.

2.1.5   Membrane Gas Absorption

Membrane gas absorption (MGA) describes a process in which gas and liquid come into contact with one another. MGA relies heavily on the use of a microporous hollow fibre membrane (Figueroa & Cuenca, 2018). The gas is being pumped through the membrane, and at the same time, a stream of absorption liquid is being pumped through the membrane on the opposite side. Compared to other methods of reducing CO_2 emissions, membrane gas absorption (MGA) offers the lowest running costs, simplicity to implement and ability to run at room temperature (Chang et al., 2022). To achieve separation, a membrane contactor combines mass transfer with the conventional phase contacting operation. Due to this property, membrane contactor procedures can be devised employing the same phenomenological strategy as conventional extraction or absorption methods. During the design of these membrane processes, one of the most important factors to consider is the optimization of the contact surface area available for mass transport through an interface while preserving a minimal pressure drop in the membrane modules (Figueroa & Cuenca, 2018).

In summary, there are various CO_2 removal technologies such as absorption, adsorption, cryogenic distillation, membrane separation and membrane gas absorption. The comparison of CO_2 removal technologies is shown in Table 2.1.

Table 2.1: Comparison of CO_2 removal technologies (Figueroa & Cuenca, 2018)

Separation technology	Advantages	Limitations
Membrane	• Simple operation • Easy to scale-up • Regeneration process is no required	• Fouling of membrane • Low membrane life-time
Cryogenic	• Matured technology • Easy storage and transportation	• Process carried out at low temperature • High investment
Absorption	• Provide high absorption efficiency more than 90 %	• Corrosivity rate is high • High energy consumption
Adsorption	• Low operational energy and cost • Low temperature and pressure for regeneration	• High energy required for desorption • Low CO_2 selectivity
Membrane gas absorption	• High flexibility • Large interfacial area • Easy to scale-up • Small footprint • High absorption capacity	• Additional membrane resistance to mass transfer

2.2   Principle of MGA system

The membrane gas absorption (MGA) is an emerging technique for carbon dioxide capture. In MGA, membranes are used as a barrier between the gas and liquid streams, allowing for more precise regulation of the two fluids (Norahim et al., 2018). Therefore, problems associated with absorption, such as flooding and entrainment, can be avoided. In contrast to most membrane separation procedures, the membrane serves solely to provide structural stability and a large gas-liquid interface area in the membrane contactor, hence enhancing mass transfer, which is the most important factor in determining CO_2 removal performance (Zhang et al., 2013).

Membrane gas absorption involves separating a feed solution containing a solute from the receiving gas phase using either a hydrophobic or hydrophilic hollow fibre contactor. This separation is accomplished by the usage of a membrane. The solute that has to be transferred is found in the gas phase when the stripping procedure is being carried out. The ability of a membrane to be hydrophobic or hydrophilic influences whether a liquid solution or gas phase may pass through it and into the pores of the membrane, which are then filled with the appropriate substance (Figueroa & Cuenca, 2018). The passage of solutes across the membrane may be accomplished by following the procedures outlined in the following sequence, which can be found in Figure 2.3.
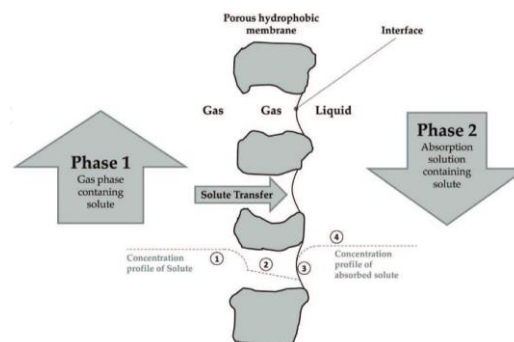
Figure 2.3: Outline of the membrane absorption process in a membrane (Figueroa & Cuenca, 2018)

Figure 2.3 depicts solute movement via a gas-phase boundary layer at the membrane surface. It is crucial to keep the feed solution on the membrane surface and the gas phase contained in the membrane pores in a state of phase balance while

employing a superomniphobic membrane. A significant amount of the absorbed solute is transferred to the receiving liquid phase. The mass transfer resistance that is encountered by CO_2 as it diffuses from the gas phase through a permeable membrane and into the liquid phase is negligible. However, if the membrane pores are completely or partially filled with a solvent, this will result in a significant increase in the resistance to the movement of mass (Norahim et al., 2018). Therefore, membranes that are suitable for membrane gas absorption should contain the characteristics of superomniphobic in order to prevent membrane wetting and excessive mass transfer resistance. A high overall porosity to minimise membrane resistance and a high chemical resistance to withstand the powerful solvent are normally used as the absorbent for CO_2 (Zhao et al., 2016).

A model based on a resistances-in-series method performed on the membrane's proximity can be used to characterise this solute transfer throughout the membrane absorption process (Estay et al., 2013). Eq. 2.1 can be used to explain the overall solute transfer via the porous membrane (Figueroa & Cuenca, 2018).

$$N_i = KA \Delta C^i_{ml} \tag{2.1}$$

where N_i represents the flux of solute that is transferred from the gas phase to the absorption phase, K represents the overall mass transfer coefficient, A represents the surface area that is available for mass transfer, ΔC^i_{ml} represents the logarithmic mean driving force in the absorption phase.

In a membrane contactor, gas and liquid are separated by porous membranes. Mass transfer via a porous membrane is seen in Figure 2.4 (Zhao et al., 2016). There are typically three stages involved: diffusion from the liquid-membrane interface to the gas-membrane contact via the membrane pores, diffusion from the gas-membrane interface to the bulk liquid, and finally physical or chemical absorption.
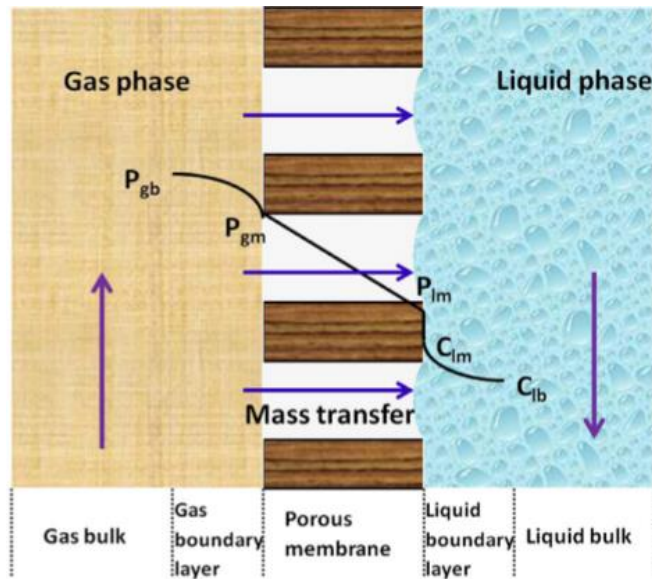
Figure 2.4: Mechanism of mass transfer in non-wetted mode through a porous membrane (Zhao et al., 2016)

2.3   Membrane Wetting Characteristics

In membrane gas absorption, it is crucial to avoid membrane wetting in order to reduce mass transfer resistance in pores. Membrane wetting happens when the liquid side operating pressure surpasses the breakthrough pressure, changing the non-wetted mode into pores that are either partially or entirely wetted, as depicted in Figure 2.5. This state imposes a substantial membrane mass transfer barrier on the gas transport and, as a result, reduces the mass transfer rate (Zhang Z.E. et al., 2014). Non-wetting operation mode is favoured because its gas-filled pores permit rapid mass transfer between gas and liquid absorbent. In this scenario, superomniphobic membrane (SOM), which is highly liquid-repellent membrane, has been introduced to capture the carbon dioxide. The surface has overhanging fluorinated nanometre-sized or micrometre-sized protrusions to achieve superomniphobicity. If an aqueous or non-aqueous liquid is placed on such a surface and the surface is slanted by less than 10°, the drop assumes a nearly spherical shape and rolls off. The liquid does not moisten superomniphobic surfaces. Instead, it remains on top of the overhangs, trapping the gas underneath. This results in a nearly 100 percent liquid-to-gas contact area (Geyer et al., 2017). A high CO_2 capture rate may result from the large contact area between liquid and gas.

14
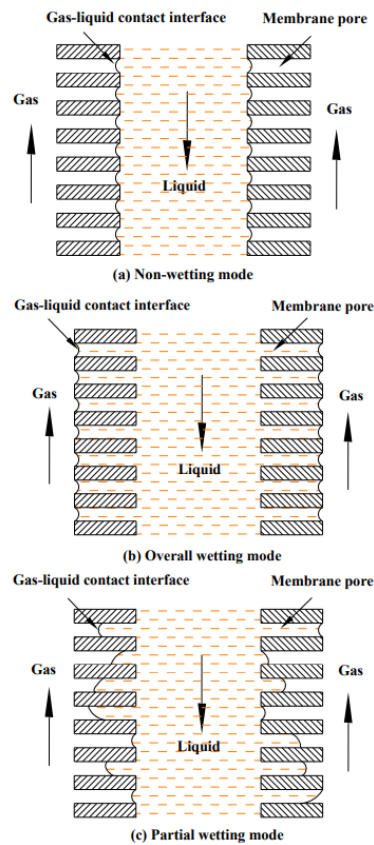
Figure 2.5: Hydrophobic hollow fibre membrane contactor operating modes (Lu, 2011)

Long-term operation of hydrophobic membranes in gas-liquid separation can cause the membrane to transition from non-wetted to partially or fully wetted. In order to lessen the tendency of membrane wetting and obtain higher operational stability, membrane hydrophobicity has evolved toward superomniphobicity. Surface is considered to be superomniphobic when it displays very high contact angles, which is approximately 150° and low roll-off angle, which is 10° for liquids with low and high surface tensions (Geyer et al., 2017). The chemical characteristics of the membrane surface free energy and membrane structure, which are hierarchical scales of texture and re-entrant texture, both have an impact on the membrane's wetting tendency (Mosadegh-Sedghi et al., 2014).

2.3.1 Surface energy

A solid surface's wettability is influenced by its surface chemical energy and surface roughness (Chen et al., 2017). Surface energy measures the breakdown of intermolecular bonds caused by the formation of a surface (Lee et al., 2017). It has been shown that the contact angle has a negative relationship to the solid surface energy, which may be deduced from Young's law and found in Eq 2.2.

$$\cos \theta = \frac{\gamma_{SV} - \gamma_{SL}}{\gamma_{LV}} \tag{2.2}$$

where γ_{SV} represents solid–vapor interfacial tension, γ_{SL} represents solid-liquid interfacial tension and γ_{LV} represents liquid–vapor interfacial tension.

This implies that surfaces with very high surface energy tend to have lower contact angles, and surfaces with very low surface energy tend to have larger contact angles. In order to achieve high performance, surfaces with low surface energy should be prioritised in the design of super-repellant surfaces. The surface energies of different functional groups on a surface are found to be in the following order: CF_3, CF_2H, CF_2, CH_3 and CH_2 (Kota et al., 2014). In order to create these superomniphobic surfaces, fluorinated and perfluorinated materials, such as fluorinated monomers, copolymers and other fluorinated precursors, have become the materials of choice.

2.3.2 Cassie-Baxter and Wenzel state

The wettability of a liquid on a rough surface may vary greatly from its wettability on a smooth one. Depending on the surface texture, a liquid droplet can enter either Wenzel state or Cassie-Baxter (CB) state, both of which include a significant reduction in the free energy required to retain the droplet's current shape (Kota et al., 2014). Cassie-Baxter model has been used to describe the relationship between the solid and gas fraction or the areal proportion of the liquid-solid and liquid-vapor interfaces as well as the apparent contact angles of a suspended liquid (Liu et al., 2015). When a liquid is in a Cassie-Baxter condition and suspended on surface

microstructures, the retreating contact line is the key factor deciding the contact-angle hysteresis.

Figure 2.6 demonstrates the system in the Cassie–Baxter condition. The liquid does not entirely wet the surface texture. Instead, air bubbles continue to be trapped underneath the liquid droplet in their own pockets (Kota et al., 2014). Liquid permeates the surface texture until the local texture angle for the three-phase contact line equals the equilibrium contact angle, as indicated by Young's relation. The Cassie–Baxter relation which is described in Eq 2.3, may be utilised to calculate the apparent contact angles under this condition.

$$\cos \theta^* = f_{SL} \cos \theta + f_{LV} \cos \pi = f_{SL} \cos \theta - f_{LV} \tag{2.3}$$

where f_{LV} represents the area fraction of the liquid–air interface underneath the liquid droplet on a surface with uniform roughness and f_{SL} represents the solid–liquid interface's area fraction.
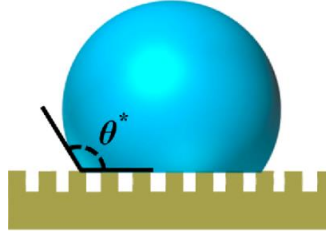
Figure 2.6: Drop liquid in the Cassie-Baxter state (Cao et al., 2015)

The Wenzel model, on the other hand, is utilised to depict a surface in which droplets penetrate the rough structures, resulting in strong adhesive forces (Kamaraj et al., 2015). A droplet that is placed on a rough surface will penetrate the rough grooves of the surface and will demonstrate a strong adhesive force between the liquid and the solid surfaces, as seen in Figure 2.7. Wenzel proposed an equation that considers the surface roughness to describe the wetting on textured surface. In equation 2.4, the correlation between roughness and contact angle is described.

$$\cos \theta_w = r \cdot \cos \theta_\gamma \tag{2.4}$$

17

where roughness, denoted by r, is defined as the ratio of the actual surface area to the projected one.
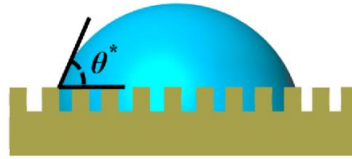
Figure 2.7: Drop liquid in the Wenzel state (Cao et al., 2015)

Contact angle on rough solid surface is different from contact angle on ideal solid surface due to the direct effect of surface roughness on the functions and effects of solid-gas interface tension and solid-liquid interface tension on system energy. Assuming that a droplet can completely fill a groove, a non-composite wetting state is produced between the droplet and the groove and the actual solid-liquid contact area is always greater than the apparent geometric contact area. As a result, the surface roughness factor is always greater than one. When the intrinsic contact angle is greater than 90°, the roughness factor increases hydrophobicity, whereas when the contact angle is less than 90°, the rough structure increases hydrophilicity (Cheng et al., 2018).
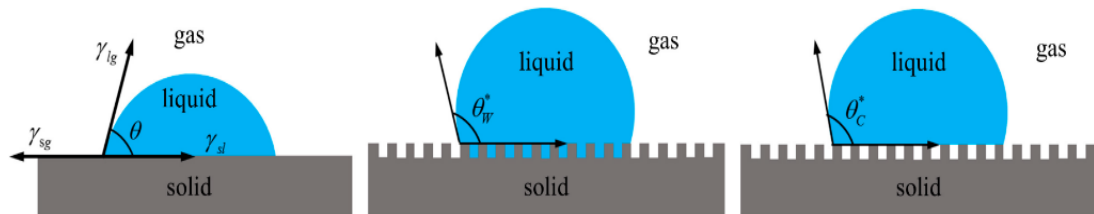
Figure 2.8: Schematic representation of (a) Young, (b) Wenzel and (c) Cassie-Baxter states of liquid droplets (Han et al., 2019)

2.3.3   Hierarchical surface

Surfaces that are impermeable to liquids tend to have a hierarchical structure, which indicates that there are multiple roughness scales (Cao et al., 2015). Hierarchical morphology is found in the shapes of many natural objects, including shark skin and lotus leaves. The surfaces of these natural objects often display an extremely high

degree of non-wettability (Jiao et al., 2018). Studies show that the presence of hierarchical structures on a surface might decrease the sliding angle and the contact angle hysteresis. The contact angle (CA) and the sliding angle (SA) of a liquid droplet on a surface are the essential components that contribute to superomniphobicity (Lei et al., 2014).

Surfaces that are hierarchically constructed often have a texture with a finer length scale that is layered on top of a texture with a coarser length scale that lies underneath it (Chamani et al., 2021). Since a liquid droplet in touch with a hierarchically structured surface is maintained in the Cassie-Baxter state throughout all length scales, the droplet's apparent contact angle tends to be larger than it would be with a smooth surface (Kota et al., 2014). This is because air is trapped at multiple length scales for a hierarchically structured surface as illustrated in Figure 2.9. Whereas, for surfaces with a single scale of texture, air is only trapped at a single length scale which will result in small apparent contact angle.
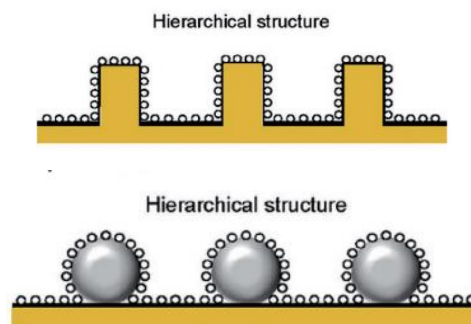
Figure 2.9: Illustrations of a drop of liquid in the Cassie-Baxter phase on a hierarchical structure (Cheng et al., 2018)

Hierarchically structured surfaces have reduced contact angle hysteresis compared to surfaces with a single scale of texture. This is because hierarchically structured surfaces may support a contacting liquid droplet in the Cassie–Baxter state. The resistance to the movement of a droplet can be characterised by a property known as the contact angle hysteresis, which is related to the energy barriers that a droplet of liquid must overcome as it moves over a solid surface (Kota et al., 2014). In this situation, there is less solid–liquid contact area, which will reduce the contact line

pinning. Therefore, hierarchically structured surfaces will exhibit small contact angle hysteresis.

2.3.4 Re-entrant surface

According to studies, membranes with re-entrant structures have decreased wetting tendency (Li et al., 2020). In the re-entrant surface, the liquid-solid-vapour interface is in a thermodynamically metastable Cassie-Baxter state as the cross-section of the solid fraction reduces towards the base of the surface (Chamani et al., 2021).

In order to maintain the Cassie-Baxter phase transition, Young's contact angle must be larger than the texture angle (Cao et al., 2015). This is because the liquid will be able to imbibe into the solid texture easily and reach a fully wetted Wenzel state if Young's contact angle is smaller than the texture angle. Therefore, as can be seen in Figure 2.10, liquids with low surface tension cannot be in a stable Cassie-Baxter condition on textures with a texture angle higher than 90° (Kota et al., 2014). Nonetheless, on textures with a texture angle of less than 90°, they can be in a Cassie-Baxter condition. The term "re-entrant texture" is used to describe such convex topographies in which the texture angle is smaller than 90°. The development of superomniphobic surfaces requires the use of re-entrant texture.

Figure 2.10: The critical role of re-entrant texture (Kota et al., 2014)

2.4 Summary of Literature Review

The summary of literature review is shown in Table 2.2. It is found that surface fluorination, silica nanoparticles and low surface energy materials are used to achieve superomniphobicity. Majority of the past researchers did not use silica nanoparticles or use different type of silica nanoparticles.

Table 2.2 Summary of Literature Review

No.	Polymer/ Powder	Inorganic filter	Solvent	How to achieve superomniphobic	Result on superomniphobicity	Application/ Research gap	Reference
1.	Pristine PVDF membrane	SiNPs	Acetone containing 1.0% (w/v) NH₂ SiNPs	• A hierarchical re-entrant architecture was created by immobilizing spherical silica nanoparticles onto a poly(vinylidene fluoride) membrane surface via covalent bonds. • The surface fluorination was achieved via thiolene click reaction to lower the membrane surface energy.	High contact angle: $166.5 \pm 1.4°$ Low sliding angle: $5.0 \pm 1.1°$	Its application is for robust membrane distillation. Different polymer and solvent are used.	(Li, Feng, Li, & Zhang, 2022)
2.	polyvinylidene fluoride (PVDF-F) membrane	-	Solution containing 4 mL of TEOS, 20 mL of 8% PVDF-O	• The fluorination of the PVDF membrane (PVDF-F) changed the surface property to superomniphobic. • Superomniphobicity chemical vapor deposition was performed at 100 °C inside the vacuum oven in the presence of TFS solution.	Contact angle: around 150° for polar solvents and low surface tension liquids	Its application is for treatment of real produced water. Different polymer and solvent are used.	(Chiao, Cao, Ang, & Sengupta, 2022)

Table 2.2 Summary of Literature Review (Cont.)

No.	Polymer/ Powder	Inorganic filter	Solvent	How to achieve superomniphobic superomniphobicity	Result	Application/ Research gap	Reference
3.	Polydimethyl siloxane (PDMS) pillars	-	Solutions of 1H,1H,2H,2Hheptade cafluorodecyl polyhedral oligomeric silsesquiox ane (F-POSS)	• The high degree of fluorination makes F-POSS one of the lowest-surface-energy molecules available. Spraying low-surface-energy polymers can lead to a controllable re-entrant texture with oleophobic properties.	For liquids with very low surface tension, such as ethanol, the ultra-low contact angle hysteresis, CAH Φ* is smaller than 3° and contact angle more than 150° is achieved.	Its application is for coatings for windows, phones, tablets, and computer screens.	(Golovin, Lee, Mabry, & Tuteja, 2013)
4.	Polyester fabrics in a solution of fluorodecyl POSS+ fluoroalkyl silane in ethanol	-	Solution of fluorodecyl POSS+ fluoroalkyl silane in ethanol	• Superomniphobic surfaces is fabricated by dip-coating polyester fabrics in a solution of fluorodecyl POSS+ fluoroalkyl silane in ethanol. • Of all the perfluorinated materials, FluoroPOSS (Fluorinated Polyhedral Oligomeric SilSesquioxanes) molecules have the lowest surface energy materials.	The dip-coated fabrics displayed very high apparent contact angles with a wide variety of liquids, including toluene (θ*=159°) and hexadecane (θ*=156°, α =6°). The surfaces were reported to be stable against UV for 24 h and against concentrated sulfuric acid.	Its application is for lightweight superomniphobic aerogels. Different polymer and solvent are used.	(Kota, Kwon, & Tuteja, 2014)

Table 2.2 Summary of Literature Review (Cont.)

No.	Polymer/ Powder	Inorganic filter	Solvent	How to achieve superomniphobic	Result on superomniphobicity	Application/ Research gap	Reference
5.	Polyvinylidene fluoride (PVDF)	SiNPs	Immersion in FAS/n-hexane solution	• The spherical geometry of the SiNPs contributes to the formation of a nano-level, the third step in the hierarchical structure yielding a superomniphobic membrane (SOM). • Surface fluorination resulted in lower surface membrane energy, ultimately achieving a superomniphobic surface that yield surface repellency and a self-cleaning property.	Contact angle (CA) values of $160.8 \pm 2.3°$ and $154.3 \pm 1.9°$ for water and oil were obtained, respectively. while 5 mM SDS and ethanol showed high and stable CA of $148.3 \pm 1.6°$ and $118.7 \pm 2.2°$, respectively.	Its application is for low surface tension oily wastewater hypersaline oily wastewaters using direct contact membrane distillation (DCMD).	(Kharraz, Farid, & Khanzada, 2020)
6.	Nickel substrates in ethanol solution	-	60 mL ethanol solution including 0.1 g NiSO4, and 0.22g TAA	• A facile hydrothermal method was used to fabricate superomniphobic coating. • The substrate was covered with dense Ni3S2 nanowires after hydrothermalreaction.	The modified coating was significantly resistant to water droplets (3μL) and the contact angle was up to 162.51°. Glycerol droplets (3μL) also remained spherical shape on its surface and the contact angle was 154.94°.	Its application is for tape-peeling and air environment. Different polymer and solvent are used.	(Yin, Yu, Hu, & Zhou, 2019)

CHAPTER 3

METHODOLOGY

3.1   Overview

This chapter discusses the materials, equipment, experimental flow, procedures and characterization techniques for fabrication of PVDF-HFP silica superomniphobic membrane. The materials used for the completion of this study are provided in Section 3.2. Section 3.3 highlights the research flow with respect to objectives 1,2 and 3. Detailed experimental procedures for the enhancement of membrane superomniphobicity are given in Section 3.4. Design of experiments are provided in Section 3.5. While, Sections 3.6 and 3.7 describe the membrane's characterization techniques and membrane gas absorption procedures, respectively.

3.2   Materials and Equipment

The materials used in membrane synthesis and characterization are discussed in this section.

3.2.1   Chemicals

Table 3.1 summarizes the details of chemicals used in this study. All chemicals are of analytical grade and used as received without further purifications.

Table 3.1: List of chemicals

No	Chemical	Properties		
		CAS Number	Purity	Supplier
1.	Polyvinylidene fluoride-co-hexafluoropropylene (PVDF-HFP)	9011-17-0	N/A	Sigma Aldrich
2	*N*-Methyl-2-pyrrolidone (NMP)	872-50-4	≥ 99.5%	Sigma Aldrich
3	Ethanol	64-17-5	≥ 95.0%	Sigma Aldrich
4	Sodium hydroxide (NaOH) aqueous solution	1310-73-2	≥97.0%,	Sigma Aldrich
5	3-aminopropyltriethoxysilane (APTES, 99%)	919-30-2	99%	Sigma Aldrich
6	Silica NPs (SiNPs, LUDOX HS-40 colloidal silica)	7631-86-9	40 wt. % suspension in H_2O	Sigma Aldrich
7	Acetate buffer	126-96-5	pH 6	Sigma Aldrich
8	FAS 1H,1H,2H,2H-Perfluorooctyltriethoxysilane (98%)	51851-37-7	98%	Sigma Aldrich
9	N-Hexane	110-54-3	≥99%	Sigma Aldrich
10	<30 nm (DLS), triethoxylpropylaminosilane functionalized (NH_2 functionalized NPs)	791334	N/A	Sigma Aldrich
11	N-Dimethylacetamide (DMAC)	127-19-5	99%	Sigma Aldrich
12	Monoethanolamide (MEA)	141-43-5	≥ 99.5%	R&M Chemicals

3.3   Experimental Flow

In this study, several project activities were carried out to achieve the research objectives. The activities flow chart was presented in Figure 3.1.
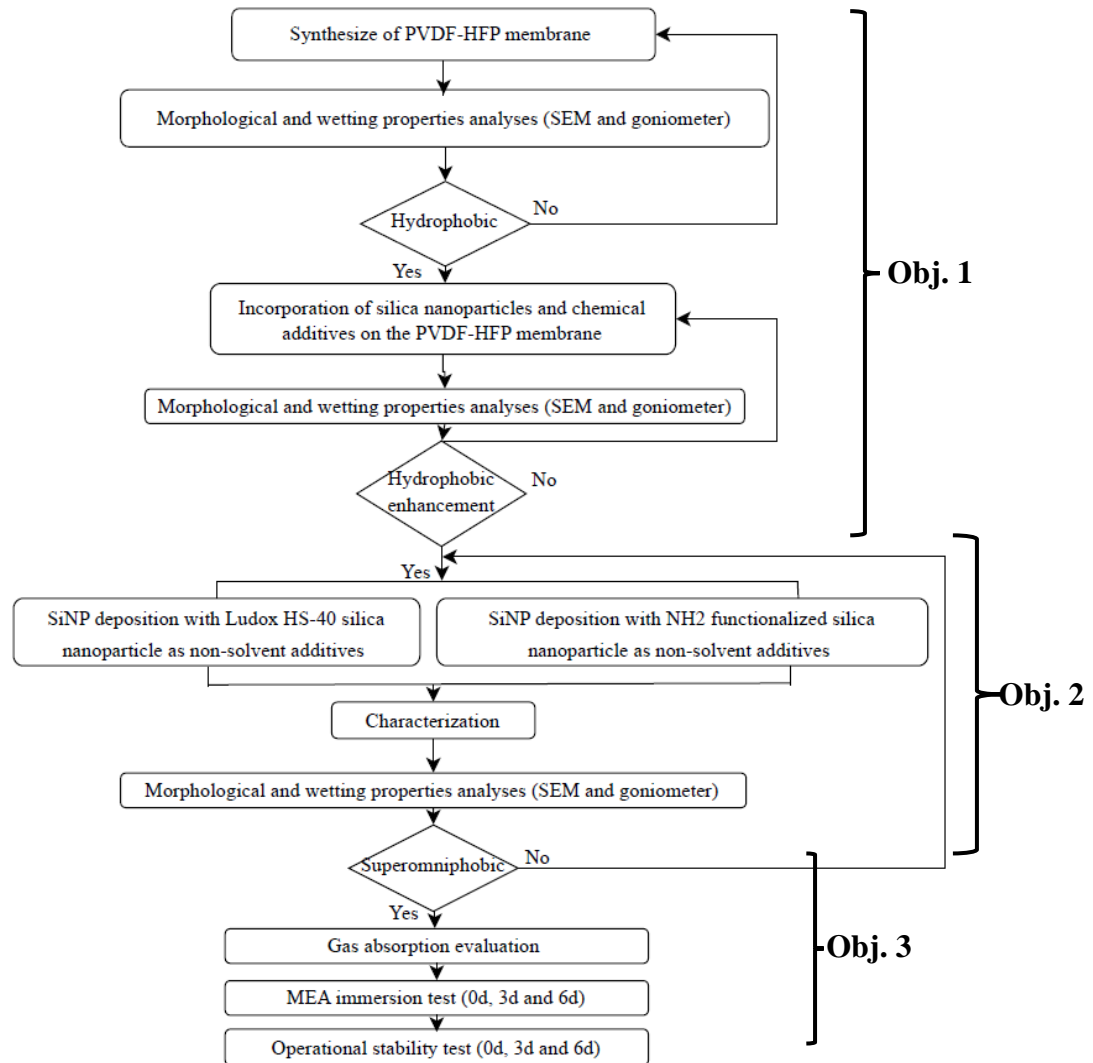
Figure 3.1: Flow chart of project activities

The experiment flow was designed based on the three objectives. For objective 1, the influence of silica nanoparticles and chemical additives on membrane superomniphobicity was evaluated. Objective 1 involved the synthesis of membrane with improved surface superomniphobicity by incorporating silica nanoparticles and chemical additives. In addition, membrane morphology and wetting properties were analysed using various characterization techniques. These included Scanning Electron

Microscopy (SEM), Energy Dispersive X-ray (EDX), Goniometry and Gravimetric Analysis. For objective 2, the order of silica nanoparticles addition on membrane superomniphobicity was evaluated. For objective 3, membrane gas absorption test was conducted to measure the membrane's CO_2 absorption performance. Prior to the gas absorption test, the membrane was immersed in MEA solution for 0, 3 and 6 days to determine its operational stability.

3.4   Experimental Procedures

Detailed experimental procedures for the development of membrane superomniphobicity are described in this section.

3.4.1   Fabrication of PVDF-HFP Membrane

The membrane was fabricated via non-solvent induced phase separation (NIPS) process. 15wt% (or 1.65g) of PVDF-HFP pellets were dried in vacuum oven at 70°C for 12 h to remove moisture. Afterwards, the polymer pellets were dissolved in 85wt% (or 9.07ml) of NMP solvent at 70°C by stirring until homogenous solution was obtained. The dope solution was degassed in ultrasonic bath for 5 h to remove trapped bubbles and left standing overnight. The polymer dope solution was poured onto a clean glass substrate and cast using a casting blade at 200 μm thickness gap. Then, the membrane film was immersed in ethanol bath immediately for 24 h to induce solvent/non-solvent exchange. This was followed by immersion in distilled water bath for 30 min to remove residue solvent. Finally, the membrane was dried in ambient condition for 48 h. The PVDF-HFP membrane was denoted as M-O. The schematic diagram for fabrication of PVDF-HFP membrane is shown in Figure 3.2.
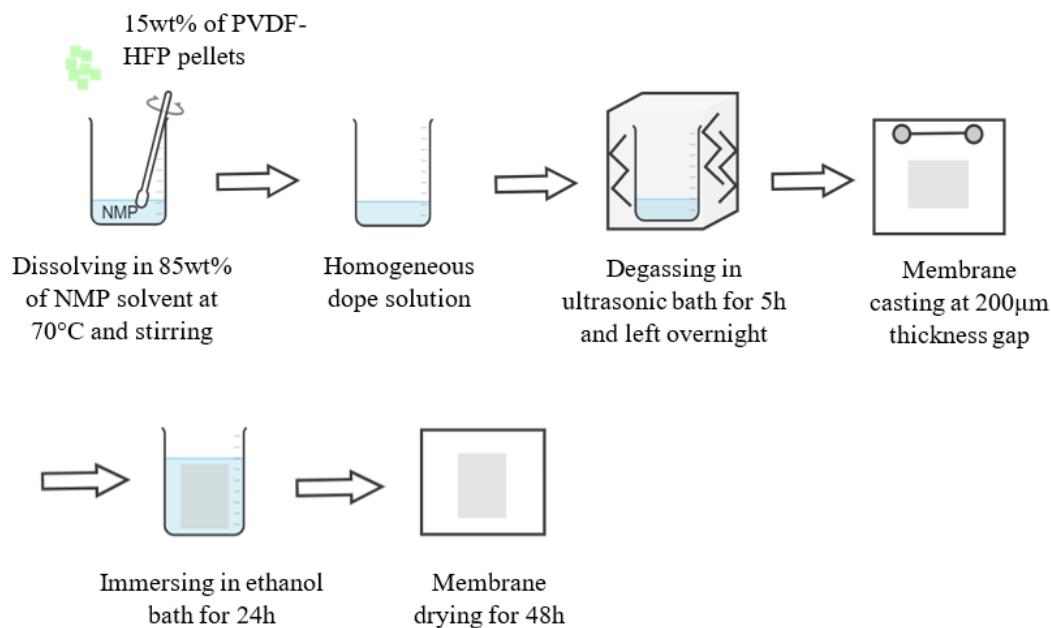
Figure 3.2: Schematic diagram for fabrication of PVDF-HFP membrane

3.4.2 Incorporation of Silica Nanoparticles and Chemical Additives on PVDF-HFP Membrane

PVDF-HFP membrane was wetted with ethanol and alkaline-treated by immersion into a 7.5 M NaOH aqueous solution at ~70 °C for 3 h to functionalize the surface with the necessary hydroxyl groups. The membrane was then washed with DI (deionized) water and dried overnight. The corresponding membrane was denoted as M-NaOH. Another PVDF-HFP membrane was immersed into a 3% v/v APTES/ethanol at ~60 °C for 1 h to functionalize the surface with amine groups, which resulted in amino functionalized membrane. The membrane was then washed with DI (deionized) water and dried overnight. The corresponding membrane was denoted as M-E. Another PVDF-HFP membrane was immersed into a 0.06% (wt.) LUDOX HS-40 SiNPs suspension prepared in a pH 6 acetate buffer for 1 h to reinforce an electrostatic attraction between the membrane and the SiNPs, yielding an SiNPs-patterned membrane. The membrane was then washed with acetate buffer and DI

(deionized) water and dried overnight. The corresponding membrane was denoted as M-L1.

Another PVDF-HFP membrane was immersed into a 0.06% (wt.) NH_2 functionalized SiNPs suspension prepared in a pH 6 acetate buffer for 1 h to reinforce an electrostatic attraction between the membrane and the SiNPs, yielding an SiNPs-patterned membrane. The membrane was then washed with acetate buffer and DI (deionized) water and dried overnight. The corresponding membrane was denoted as M- N1. Another PVDF-HFP membrane was fluorinated by immersing the membrane into a 1% v/ v FAS/n-Hexane at ~60 °C for 24 h, which result in a hydrolysis reaction between the membrane and FAS. The corresponding membrane was denoted as M-H. Another membrane was cast with a second layer composed of 10 wt% of PVDF-HFP dissolved in DMAc with a casting thickness of 200 μm. An imprinting was made on top of the second layer using a diamond-shaped net spacer while the layer was still liquid, and the imprinting depth was set to be 0.7 mm, which was the spacer string thickness. This was followed by an exposure of 5 minutes. After 5 minutes, the spacer was manually delaminated from the nascent membrane. The nascent membrane was then kept in the bath for forty minutes, which was followed by overnight drying in the surrounding air. The corresponding membrane was denoted as M-S.
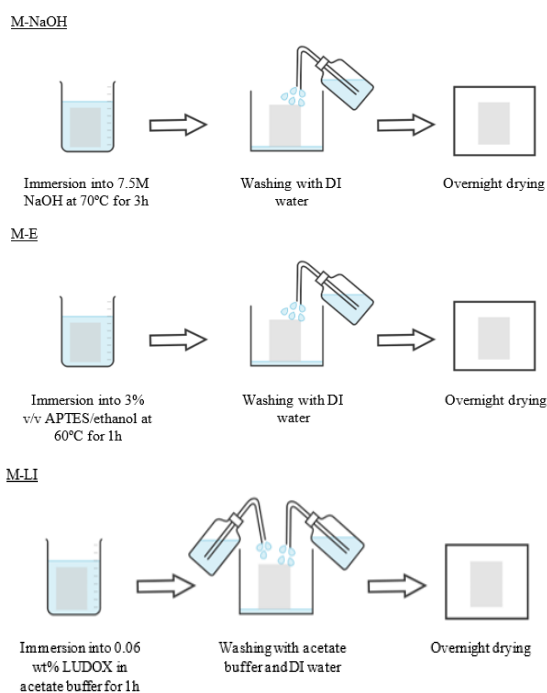
Figure 3.3: Schematic diagram for incorporation of chemical additives on PVDF-HFP membrane

M-NI

Immersion into 0.06 wt% NH₂ in acetate buffer for 1h → Washing with acetate buffer and DI water → Overnight drying

M-H

Immersion into 1% v/v FAS/n-Hexane at 60°C for 24h → Washing with DI water → Overnight drying

M-S

Prepare 10wt% PVDF-HFP in BMAc → Second layer of membrane casting at 200 μm → Imprinting by diamond shape net spacer → 5 minutes exposure

Delamination of spacer → Immersion water bath → Overnight drying

Figure 3.4: Schematic diagram for incorporation of silica nanoparticles and chemical additives on PVDF-HFP membrane

3.4.3 Incorporation of Silica Nanoparticles as Non-Solvent Additives

The procedures involved in the enhancement of PVDF-HFP membrane hydrophobicity were similar to that of PVDF-HFP membrane. 15wt% (or 1.65g) of PVDF-HFP pellets were dried in vacuum oven at 70°C for 12 h to remove moisture. Afterwards, the polymer pellets were dissolved in 85wt % (or 9.07ml) of NMP solvent at 70°C by stirring until homogenous solution was obtained. The dope solution was

degassed in ultrasonic bath for 5 h to remove trapped bubbles and left standing overnight. Coagulation bath was prepared by dispersing 0.06% (wt.) LUDOX HS-40 SiNPs and NH$_2$ functionalized SiNPs in ethanol. This solution was stirred at 300 rpm for 2 hours. The corresponding membrane was denoted as M-L2 and M-N2, respectively. The polymer dope solution was poured onto a clean glass substrate and cast using a casting blade at 200 μm thickness gap. Then, the membrane film was immersed in ethanol bath immediately for 24 h to induce solvent/non-solvent exchange. This was followed by immersion in distilled water bath for 30 min to remove residue solvent. Finally, the membrane was dried in ambient condition for 48 h.
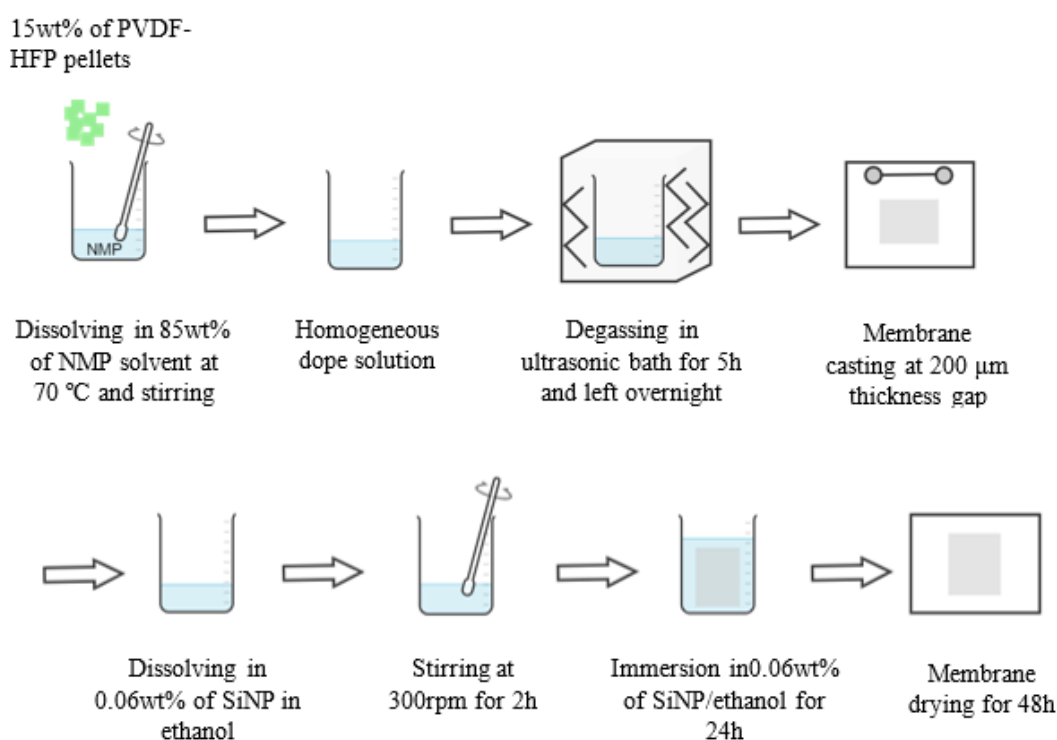
Figure 3.5: Schematic diagram for incorporation of silica nanoparticles as non-solvent additives

3.5 Design of Experiment

There are 9 samples in this project, which include the incorporation of silica nanoparticles and immersion of chemical additives. The design of experiment is used as shown in Table 3.2.

Table 3.2: Design of Experiment

Sample No.	Denotation	Polymer	Chemical or SiNP added
1	M-O		-
2	M-NaOH		7.5 M NaOH aqueous solution
3	M-E		3% v/v APTES/ethanol
4	M-L1		0.06 % (wt.) LUDOX HS-40 SiNPs
5	M-N1	PVDF-HFP	0.06 % (wt.) NH_2 SiNPs
6	M-H		1% v/ v FAS/n-Hexane
7	M-S		Diamond- shaped net spacer
8	M-L2		0.06 % (wt.) LUDOX HS-40 SiNPs (as non-solvent additive)
9	M-N2		0.06 % (wt.) NH_2 SiNPs (as non-solvent additive)

3.6 Membrane Characterization

Analysis of the morphological and wetting characteristics were carried out in order to characterise the fabricated superomniphobic membranes. Morphological analysis was carried out with Scanning Electron Microscope (SEM) and Energy Dispersive X-Ray (EDX) as shown in Table 3.3. Whereas, membrane wetting properties analysis was conducted using Goniometry as shown in Table 3.4.

3.6.1 Morphological Analysis and Wetting Properties Analysis

The morphological analysis and wetting properties analysis are shown in Table 3.3 and Table 3.4

Table 3.3: Equipment for Morphological Analysis

No.	Equipment	Brand	Purpose
1	Scanning Electron Microscopy (SEM)	Brand: Zeiss Model: Evo LS15 VPSEM	Visualize the membranes' surface and cross-section microstructure
2	Energy Dispersive X-Ray Spectroscopy (EDX)	Brand: Zeiss Model: Evo LS15 VPSEM	Analyse the elemental composition of membrane samples

Table 3.4: Equipment for Wetting Properties Analysis

No.	Equipment	Brand	Purpose
1	Goniometry / Optical Contact Angle Measurement Instrument (OCA 25)	Brand: Rame-Hart Model: 260	Measure contact angles (CAs) with water and MDEA

3.7   Membrane Gas Absorption Evaluation

The tests for CO_2 gas absorption were carried out at ambient temperature and pressure. The membrane module was filled with a membrane sample. The mass flow metre maintained the flow rate of the gas at a constant 150 mL/min. As illustrated in Figure 3.5, a peristaltic pump was utilised in the process of pumping the liquid absorbent, which was 1.5 M of MEA solution, into the other side of the membrane module at a rate of 150 mL/min. After 30 minutes of operation when the system reached a steady state, a bubble flow metre was utilised to measure the outlet CO_2 gas flow rates. By subtracting the exit gas flow rate from the inlet gas flow rate, the total CO_2 absorption flux, J ($molm^{-2}s^{-1}$), was determined.
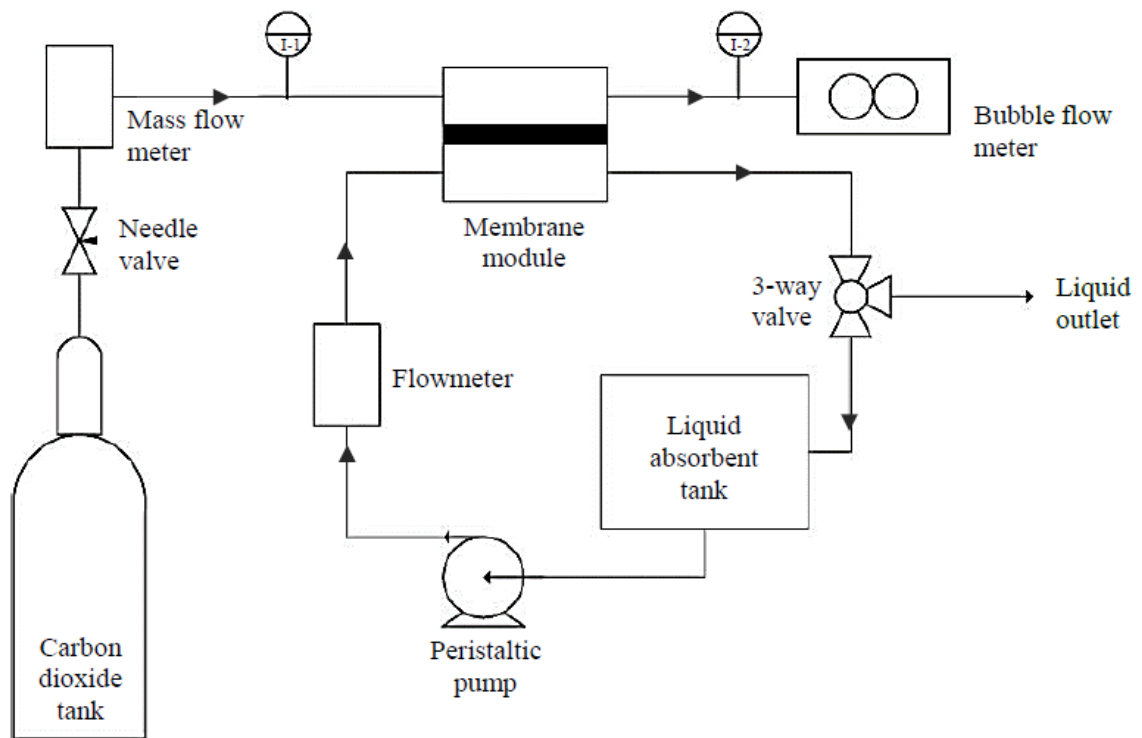
Figure 3.6: Schematic diagram of membrane gas absorption

CHAPTER 4

RESULTS AND DISCUSSION

4.1   Overview

This chapter provides the findings from the conducted experiment and rationalization. In Section 4.2, the influence of silica nanoparticles and chemical additives on membrane morphology and hydrophobicity was discussed. Section 4.3 discusses the order of silica nanoparticles on membrane superomniphobicity. Meanwhile, Section 4.4 elucidates the gas absorption performance of synthesized membrane.

4.2   Influence of Silica Nanoparticles and Chemical Additives on Membrane Superomniphobicity

The influence of silica nanoparticles and chemical additives on membrane morphology and superomniphobicity was discussed.

4.2.1   Morphology Analysis

SEM analysis was conducted to provide a visualization of the membrane structure as shown in Figure 4.1. Figure 4.1 (a) shows that the surface of the membrane consisted of particulate-like structure. The semi-crystalline PVDF-HFP polymer globules were used to form this structure, which are interconnected to each other. Similar structure was seen in a PVDF membrane study by Ahmad and colleagues when soft non-solvent was

employed (Ahmad & Ramli, 2013). The polymer particles interconnected to form particulatemorphology dominated by crystallization-controlled phase separation. This was the result of soft precipitation baths like alcohols retarded the precipitation rate and permitted a larger degree of solid-liquid demixing (crystallisation) to take place during the immersion process. This is attributed to the high thermodynamic stability and low diffusion coefficient (Liu et al., 2018). By referring to cross-section morphology in Figure 4.1 (b), the crystallizable segments of PVDF-HFP caused the formation of nodular crystalline particles during the solid-liquid demixing process. During this process, all of the polymer particles nucleated to a comparable size and fused together to form an interconnected-particulate structure in the membrane. This led to the observation of crystallization-controlled phase separation that occurred in the process. This finding is in good agreement with the research work done by Hamzah and Leo (Hamzah & Leo, 2017). They mentioned that such a morphology could increase the surface roughness of membranes, which would make membrane surfaces to be more omniphobic (Hamzah & Leo, 2017).

It is observed that Figure 4.1 (c) shows a denser top surface microstructure compared to that of Figure 4.1 (a). It is due to the immersion of PVDF-HFP membrane in APTES/ethanol bath. As a result of a slower vapour uptake rate during immersion in the APTES-ethanol solution, the morphology reveals the predominance of PVDF-HFP crystal spherulites. This allowed the PVDF-HFP crystal nuclei to develop radially and produce such spherulites (Abdulla AlMarzooqi et al., 2017). The cross-sectional morphology of the membrane in Figure 4.1 (d) reveals that exposure to a soft precipitation bath led to the formation of a symmetric structure in the membrane, which was accompanied by a reduction in the size of the macrovoids. A significant number of spherulites clumped together and were dispersed uniformly throughout the entirety of the membrane. This is corroborated by the findings of Buonomenna et al., who discovered that the use of alcohols as a non-solvent enhanced the creation of a bi-continuous structure formed of nucleated crystalline particles (Buonomenna et al., 2007).

Figure 4.1 (e) shows the top surface SEM image of PVDF-HFP membrane after immersion in FAS/n-hexane for 24 hours. It is observed that the membrane shown in

Figure 4.1 (e) shows a membrane with high surface roughness. When a membrane's surface has a high degree of corrugation, the space between the corrugations becomes too small for hydrogen-bonded water molecules and other liquid molecules to pass through and permeate the rough surface. As a result, it is projected that it has a high level of wetting resistance (Kota et al., 2014). The cross-sectional microstructure of M-H membrane shows the symmetric structure which is similar to the M-0 membrane, the pristine membrane. By referring to cross-section morphology, it is found that the FAS/n-hexane was embedded in the skin layer of PVDF-HFP membranes as it did not change the cross-sectional microstructure of the membrane as shown in Figure 4.1 (f).
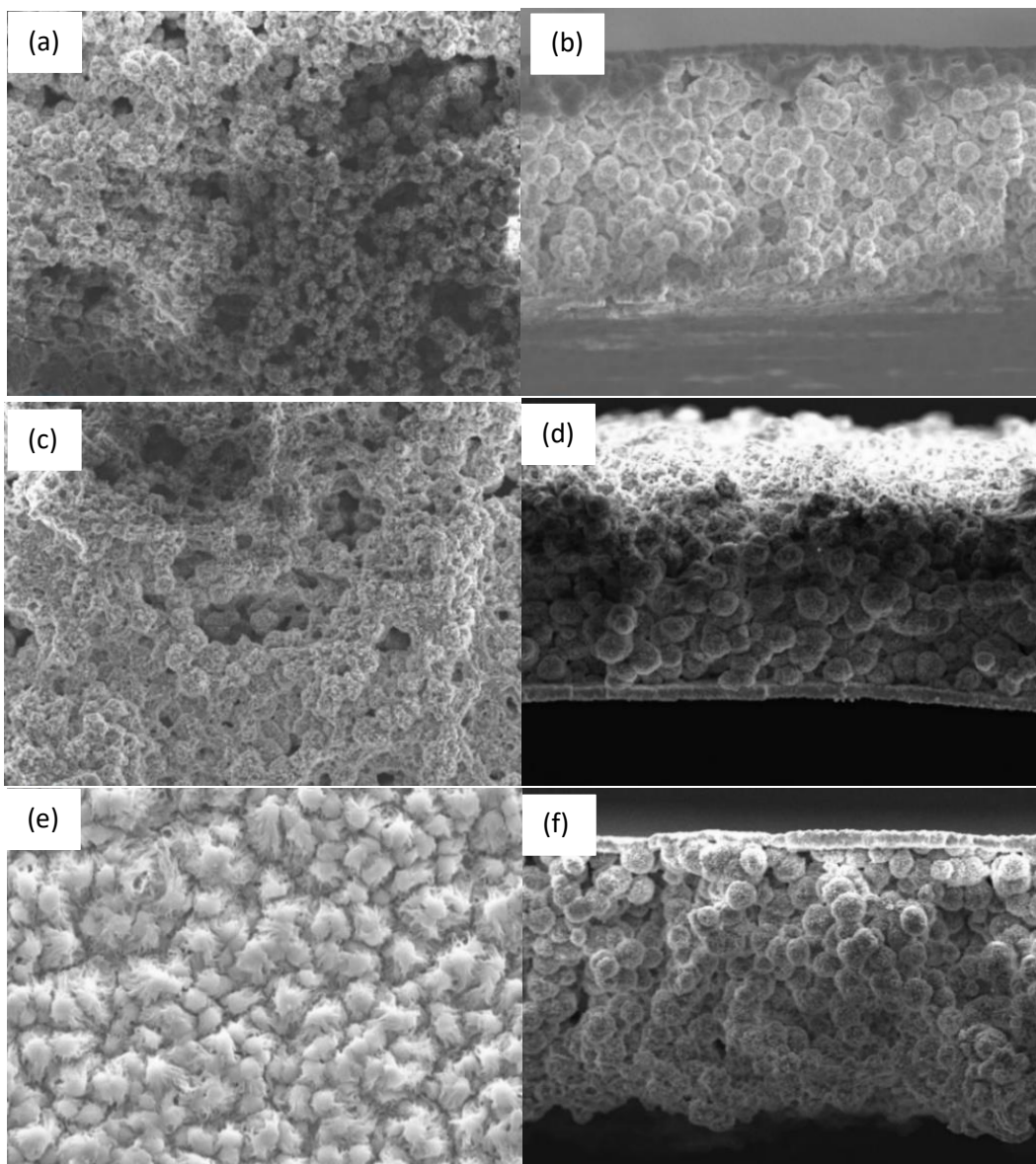
Figure 4.1: Top surface and cross-sectional SEM images of (a, b) M-O, (c, d) M-E and (e, f) M-H membranes

4.2.2 Elemental Analysis

The presence of carbon (C) and fluorine (F) on membranes was examined by EDX analysis, as summarized in Table 4.1. These membranes represent PVDF-HFP polymer with 3% v/v APTES/ethanol (M-E) and 1% v/ v FAS/n-Hexane (M-H) respectively.

Table 4.1: Elemental analysis of membrane surface

Membrane sample	Elemental analysis (wt %)	
	C	F
M-E	54.38	37.07
M-H	52.75	46.50

For M-E membrane, 54.38 wt % of C content and 37.07 wt % of F content are detected on the membrane as shown in Table 4.1. Whereas, 52.75 wt % of C content and 46.50 wt % of F content are detected on the M-H membrane. As shown in Figure 4.2, an increment of 9.43 wt % in the F is determined due to the fluorination of M-H membrane in 1% v/ v FAS/n-hexane. Such disparity in F intensity suggests an enhanced fluorination on the M-H membrane surface.

It is anticipated that the weight percentage increase in fluorine result in an improvement of the superomniphobicity of membrane. As reported by Di et al., fluorinated materials typically exhibit both oleophobicity and hydrophobicity at the macroscopic level (Di et al., 2022). It was proposed that the surface free energy of the chemical group followed the sequence CF_3, CF_2H, CF_2, CH_3 and CH_2 (Kota et al., 2014). In addition, Wang and co-workers observed that the CF_3 group exhibited the lowest surface free energy of all chemical groups (Wang & Gong, 2017). This is due to the comparatively low surface energy that fluorinated materials possess (Di et al., 2022).
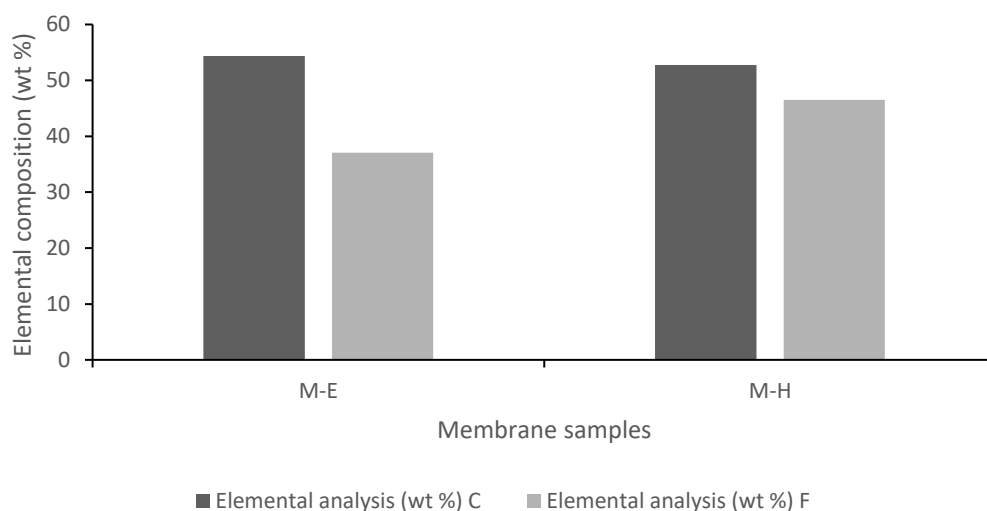
Figure 4.2: Elemental analysis of membrane surface

4.2.3 Contact Angle Analysis

Water contact angle (CA) measurement and 50 wt% tertiary alkanolamine N-methyldiethanolamine (MDEA) contact angle were conducted using the goniometer to study the hydrophobicity of the synthesized membranes as shown in Figure 4.3 with droplet images on the membrane surface.

The pristine PVDF-HFP membrane (M-O) shows a water contact angle of 129.18 ± 1.92^{o} and MDEA contact angle of 109.60 ± 2.31^{o} as shown in Figure 4.3. The potential application of synthesized membranes was examined by measuring the MDEA contact angle on membrane surface. According to the SEM morphology, this phenomenon was attributed to the membrane's roughness, which can be seen as a bumpy surface interspersed with multiple levels of protrusions (see Figure 4.1). The finding of pristine PVDF-HFP membrane is in good agreement with the study reported by Toh et al. (2020). According to Ooi et al. and Peng et al., the skinless spherical globules shape in soft non-solvent-induced membrane showed considerable surface roughness (Ooi et al., 2012).

On the other hand, M-NaOH membrane shows low water and MDEA contact angles, which are 39.93^{o} and 23.54^{o}. It shows a reduction of 89.25^{o} in water contact angle and 86.06^{o} in MDEA contact angle compared to M-O membrane. This finding

is in good agreement with the research done by Zhang et al. (Zhang et al., 2020). They stated that the hydrophilic nature of the surface causes water molecules to be strongly attracted to the surface, resulting in high affinity for water and low contact angle (Zhang et al., 2020). According to Pratten and Craig (1989), solids with a contact angle of less than 90 degrees when water is the wetting liquid are described as hydrophilic. Therefore, M-NaOH membrane is considered to be a hydrophilic membrane. When a liquid droplet is placed on M-NaOH surface, it tends to spread out over a large area, resulting in a small contact angle. It is due to the immersion of NaOH coagulation bath. In this case, the membrane was decorated with hydroxyl functional group which results in the hydrophilic surface. According to Yao et al. (2012), hydrophilic material on the surface reduces the contact angle.

Referring to Figure 4.3, M-S membrane exhibits higher water and MDEA contact angles than M-NaOH membrane, which are 64.77° and 41.84° respectively. However, it shows a decrease in comparison to M-O membrane. This finding contradicts with the research done by Kharraz et al. (2020). It might be due to the fact that different pristine membranes are utilized in the study by Kharraz and co-researchers, which is the commercial flat sheet PVDF membrane. Whereas, in this research study, the fabricated PVDF-HFP membrane with ethanol immersion for solvent-nonsolvent exchange was used as the pristine membrane. The net spacer destroyed the morphology top surface of the PVDF-HFP membrane when the second layer of DMAC with a casting thickness of 200 μm is cast on the first layer. Meanwhile, M-N1 shows a higher water and MDEA contact angles than M-NaOH membrane, which are 108.49° and 84.88° respectively.

Besides, M-E membrane exhibits higher water contact angles than M-N1 membrane but lower MDEA contact angle than M-N1 membrane, which are 117.61° and 74.83° respectively. As shown in the surface morphology of M-E membrane, it is observed that the M-E membrane has a rough surface. According to the Cassie-Baxter model, rough surface has a greater propensity to trap pockets of air between hill and valley-like region. This results in a small surface area available to be contacted by the liquid droplet, hence a high contact angle is obtained (Darband et al., 2020). However, in comparison to M-O membrane, M-E membrane shows a reduction in water and

MDEA contact angles. It is due to the immersion of M-O membrane in APTES/ethanol in 60ºC destroys the hydrophobic and oleophobic characteristic of PVDF-HFP membrane. Thus, it is concluded that immersion of M-O membrane in APTES/ethanol is not an option to produce a superomniphobic membrane.

M-L1 membrane displays higher water and MDEA contact angles than the pristine (M-O) membrane, which are 135.99º and 126.34º respectively as shown in Figure 4.3. It shows an improvement in the omniphobocity of M-L1 membrane when compared to the contact angle of pristine PVDF-HFP. The increment in the water and MDEA contact angles is due to the incorporation of LUDOX HS-40 silica nanoparticles on the pristine membrane (M-O). The silica nanoparticles have a spherical geometry, which offers the necessary re-entrant structure and contributed to the higher wetting resistance. Nanoscale patterns were produced as a result of the spherical SiNPs being adhered to the surface of the membrane. This finding is in good agreement with the study done by Kharraz et al. (2020). As mentioned by Kharraz et al., the spaces that exist between these nano-scale neighbouring patterns are not easily filled by liquid. Instead, they are filled with air that is trapped beneath the liquid (Kharraz et al., 2020). When this occurs, the contact area between the liquid and the surface of the SOM is greatly diminished, which leads to extremely high CA values due to the fact that the liquid is repelled by the hydrophobic air that lies underneath. In addition, as reported by Zhang et al. (2012), the presence of a hydrocarbon chain due to incorporation of silica nanoparticles led to the imposition of a significant resistance on the liquid phase. As a result, the wetting resistance of the membrane was significantly improved (Zhang et al., 2012).

M-H membrane exhibits the higher water and MDEA contact angles than the pristine membrane, which are 137.50º and 133.59º respectively. By using fluorination, there is an increment of 8.32º and 23.99 º in terms of water and MDEA contact angles compared to M-O membrane. The result is in good agreement with the research done by Di et al. (2022), which mentioned that fluorinated materials often exhibit both oleophobicity and hydrophobicity at the macroscopic level due to their comparatively low surface energy (Di et al., 2022). The increment in contact angles is due to the fluorine atoms are less polarizable and have a greater van der Waals radius than other

atoms, which results in weaker van der Waals interactions between fluorinated chains and lower cohesive energy densities in liquid fluorocarbons (Molchanova et al., 2017). Since the hydrophobic impact of the chain is typically proportional to the area exposed to water, the increased hydrophobicity of fluorocarbon chains in water is partially attributable to the greater molecular surface offered by fluorination. This is explained by the substantial entropy loss caused by the creation of a network of hydrogen bonds between water molecules around the solute (Lin et al., 2018). Besides, as reported by Carlson et al., experimental and theoretical research have demonstrated that the dispersive work of adhesion decreases dramatically as fluorination increases, which result in higher contact angle of the membrane (Carlson et al., 2021).

From Figure 4.3, it is observed that the MDEA contact angle is lower than water contact angle for pristine membrane and synthesized membranes. This finding is supported by the statement of Geyer et al., who mentioned that liquids with low surface tension tend to have relatively low contact angles (Geyer et al., 2017). It is because 50 wt% of MDEA has a lower surface tension, which is 50.8 mN/m when compared with water with surface tension of 72.8 mN/m. Liquid with low surface tension could wet the membrane surface more easily as low surface tension liquids exhibit the Young's contact angle, θ less than 90°. According to a study by Ryu et al., high surface tension liquids tend to resist spreading out over the surface of a solid material, resulting in a larger contact angle (Ryu et al., 2018). This is because the cohesive forces between the molecules of the liquid are sufficient to overcome the adhesive forces between the liquid and the solid surface. This results in the liquid forming a compact droplet, which has a larger contact area with the surface. This research's finding is also supported by a study of Xu et al., which found that liquids with low surface tension had very low contact angles with solid surfaces (Xu et al., 2017).
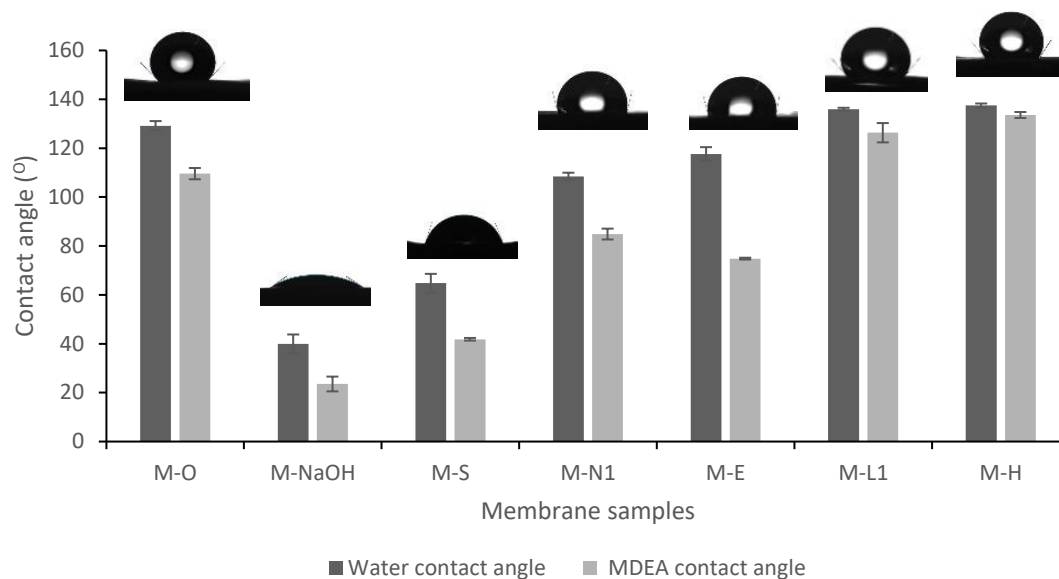
Figure 4.3: Contact angles of membranes using water and MDEA

4.2.4 Porosity Analysis

The porosity of the PVDF-HFP membrane and other synthesized membranes are determined by gravimetric analysis are shown in Figure 4.4. The pristine membrane (M-O) membrane exhibits a porosity of $62.23 \pm 3.18\%$. Other synthesized membranes have higher porosity than the pristine membrane. Among the synthesized membranes, M-L1 membrane has the highest porosity, which is $78.39 \pm 1.22\%$. It is followed by M-E, M-H and M-N1 membrane, which has $74.18 \pm 0.67\%$, $73.34 \pm 1.77\%$ and $71.68 \pm 3.32\%$ porosity respectively. It is found out that the incorporation of silica nanoparticles results in higher porosity which are exhibited by M-N1 and M-L1 membranes. The result is in good agreement by Ji and his co-workers (2018) that observed a similar porosity trend for PSF/FEP mixed matrix membrane. They emphasized that the phase separation between the polymer matrix and the dispersed phase of hydrophobic nanoparticles would cause interfacial micro voids due to the difference in hydrophobicity between the two phases (Ji et al., 2018). This was likely attributable to the steric repulsive forces exerted by silica nanoparticles, which led to a poor contact with the polymer matrix and induced a high porosity.

Other synthesized membranes such as M-NaOH, M-S, M-E and M-H membranes exhibit the porosity remained between $68.54 \pm 0.92\%$ and $74.18 \pm 0.67\%$. This demonstrated that the immersion of membranes in different chemicals do not have much effect on the porosity. A similar globular type structure was observed with the cross-sectional SEM image (see Figure 4.1) in the synthesized membrane. The immersion of membranes in different chemicals only forms a deposition layer on the membrane surface, which does not affect the cross-sectional area of the membrane. Hence, it can be concluded that chemical immersion has a lesser impact on the membrane's porosity compared to silica nanoparticles incorporation.

As shown in Figure 4.4, M-H membrane exhibits a lower porosity compared to M-L1 membrane even though the contact angle of M-H membrane is higher than M-L1 membrane. M-H membrane results in a decrement of 5.05% in porosity compared to M-L1 membrane. It is due to the dense structure exhibited by M-H membrane due to fluorination. Fluorine atoms can pack tightly together due to their small size, which can increase the overall density of the membrane structure. The membrane's dense structure lessens macro-voids, which lowers porosity (Chiam & Sarbatly, 2013). Rosnan and her colleagues emphasised the connection between the decline in porosity and the rise in viscosity, which stifled the exchange of solvent and non-solvent during phase inversion (Rosnan et al., 2018). As a result, the emergence of macro-voids was prevented, and a membrane with a denser and less porous structure was created (Fan & Peng, 2012).
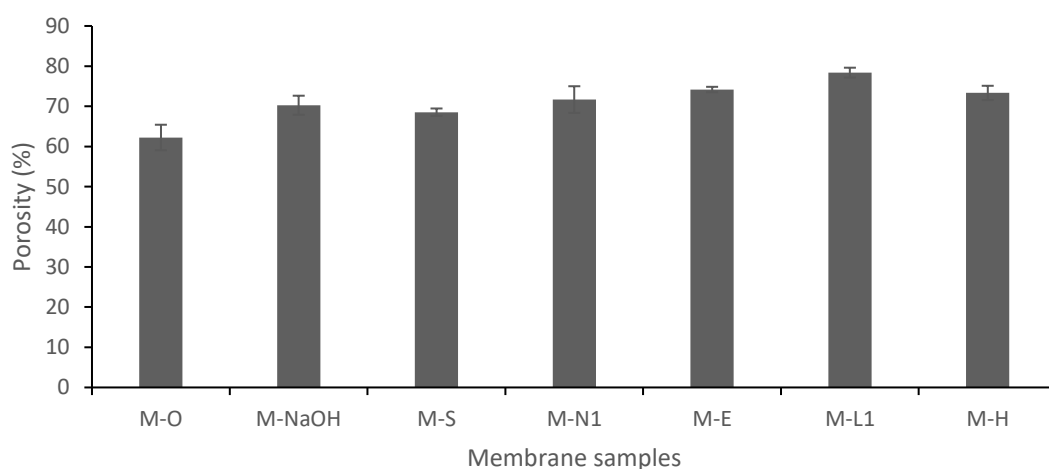
Figure 4.4: Porosity of membrane samples

4.3 Order of Silica Nanoparticles Addition on Membrane Superomniphobicity

In this section, the order of silica nanoparticles addition on membrane superomniphobicity was investigated. A comparison between membranes were also discussed in terms of morphology, elemental analysis, contact angle and porosity.

4.3.1 Morphology Analysis

In order to visualize the membrane's structure, SEM analysis was performed. As described in Section 4.2, the PVDF-HFP membrane was synthesized in an ethanol coagulation fluid. The effect of incorporation of NH_2 functionalized silica nanoparticle as non-solvent additive is shown in Figure 4.5 (a, b, c), which is denoted as M-N2. Whereas, the effect of incorporation of LUDOX HS-40 silica nanoparticles as non-solvent additives is shown in Figure 4.5 (d, e, f), which is denoted as M-L2. It is observed that the cross-sectional area of both membranes exhibits similar hierarchical nodular morphology as M-O membrane throughout the polymer matrix (see Figure 4.1). However, denser structure was observed in M-N2 and M-L2 membranes. Besides, LUDOX HS-40 silica nanoparticles have the average nanoparticle diameter of 15.11 μm, which are larger than NH_2 functionalized silica nanoparticles that have the average nanoparticle diameter of 10.08 μm.

The finding is in good agreement with the research work by Wu et al. (2018), who mentioned that when hydrophobic silica was added to the coagulation bath, it resulted in the formation of nanoparticles that were tightly attached to the membranes (Wu et al., 2018). This may be explained by the movement of silica nanoparticles from the coagulation medium onto the polymer layer that occurs concurrently with the exchange of solvent and nonsolvent. According to another study by Rana et al., this morphology is associated with the diffusional rate of solvent-nonsolvent exchange during the phase inversion process (Rana et al., 2015). The addition of hydrophobic silica nanoparticles augmented the viscosity of the polymer dope solution, thereby increasing the resistance to solvent and non-solvent exchange. This intensified the delayed phase inversion and permitted a greater extent of polymer crystallization to

take place during the precipitation process (Wu et al., 2018). Subsequently, the membrane's microstructure became denser and more compact.
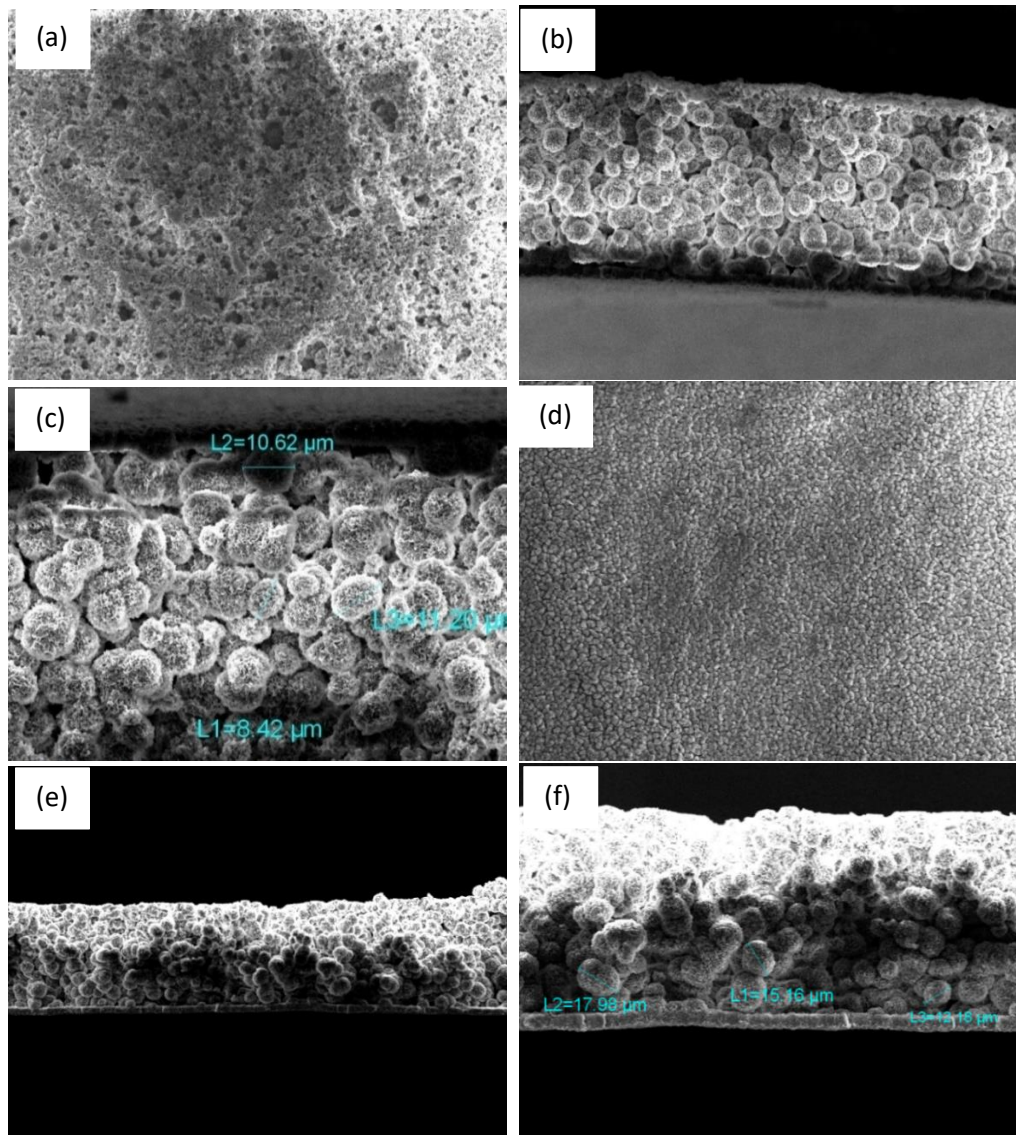
Figure 4.5: Top surface and cross-sectional SEM images of (a, b, c) M-N2 and (d, e, f) M-L2

4.3.2 Elemental Analysis

Table 4.2 summarises the results of an EDX analysis of the presence of carbon (C), fluorine (F), and silicon (Si) on the membranes. These elements represent PVDF-HFP polymer with 0.06 % (wt.) Ludox HS-40 SiNPs suspension and 0.06 % (wt.) NH2 functionalized SiNPs suspension.

Table 4.2: Elemental analysis of membrane surface

Membrane	Elemental analysis (wt %)		
	C	F	Si
M-N2	54.67	44.99	0.12
M-L2	52.51	46.46	0.36

For M-N2 membrane, 54.67 wt % of C content, 44.99 wt % of F content and 0.12 wt % of Si content are detected on the membrane as shown in Figure 4.6. Whereas, 52.51 wt % of C content, 46.46wt % of F content and 0.36 wt % of Si content are detected on the M-L2 membrane. An increment of 1.53 wt % in the F and 0.24 wt % in the Si content is determined on M-L2 membrane due to the incorporation of different silica nanoparticles. Such disparity in F and Si intensity suggested an enhanced fluorination and enhanced migration of silica nanoparticles on the membrane.

The enhanced fluorination and enhanced migration of silica nanoparticles on the membrane result in an increment of weight percent content of F and Si contact, thus increasing contact angle and improving superomniphobicity on the membrane. It is because hierarchical structure is generated between a dual-scale roughness composed of silica nanoparticles and membrane (Xiao et al., 2020). Therefore, a low surface energy of coating layer has existed on the membrane. This configuration effectively reduces the liquid-solid contact area and the likelihood of foulant interaction with the membrane surface (Bing-Bing et al., 2015). Additionally, it enlarges the evaporation area to counteract the SiNPs coating's dramatic reduction in flux (Wu et al., 2016).
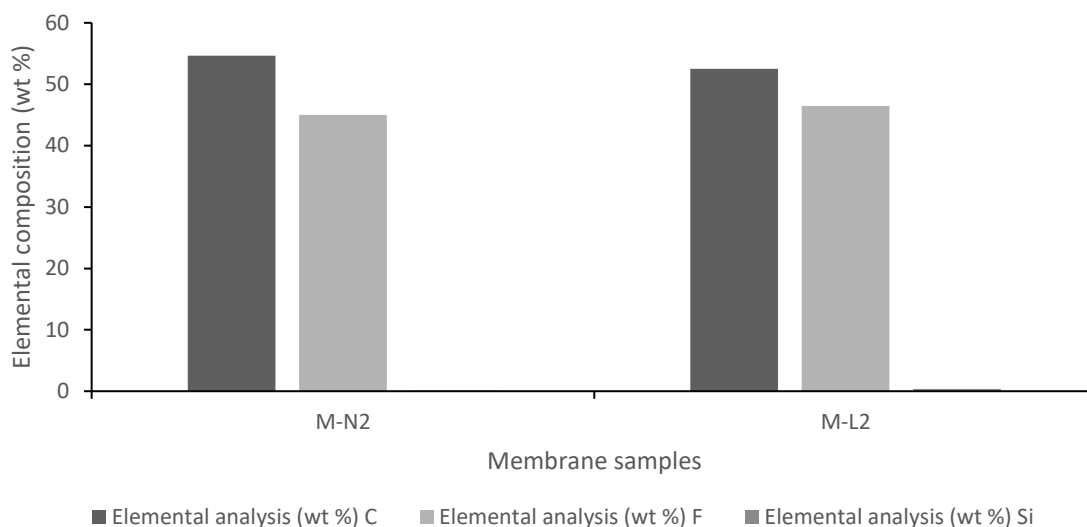
Figure 4.6: Elemental analysis of Synthesized Membrane

4.3.3 Contact Angle Analysis

Water and MDEA contact angle measurement was conducted using the goniometer to study the superomniphobicity of the synthesized membranes as shown in Figure 4.7 with the droplet images on the membrane surface. The water and MDEA contact angles exhibited by M-N2 membrane are determined to be 146.26 ± 1.42^{o} and 129.38 ± 2.03^{o}, which corresponded to enhanced wetting resistance. Upon addition of another type of silica nanoparticle, which is LUDOX HS-40 silica nanoparticle, the M-L2 membrane achieve superomniphobicity with water and MDEA contact angles exceeding 150°, which are 164.97 ± 2.81^{o} and 153.31 ± 2.13^{o} respectively. In comparison to the pristine membrane (M-O), the water contact angle is drastically improved by 13.22% for M-N2 and 27.71% for M-L2. Whereas, the MDEA contact angle is significantly increased by 18.05% for M-N2 and 39.88% for M-L2 membrane compared to the pristine membrane.

It is found that the incorporation of silica nanoparticles results in high contact angle of the membrane. This result is in good agreement with the study done by Lu et al. (2018) who highlighted that that higher contact angle of membrane is achieved after being coated with 60 nm nanoparticles on polyvinylidene difluoride (PVDF) hollow fibre membrane. It is mainly due to re-entrant surface structure generated by the

48

nanoparticle, thus increasing the membrane surface roughness (Lu et al., 2018). A qualitative analysis by Xu et al. (2021) demonstrates that the net force on the liquid–vapor interface is directed away from the solid surface for a re-entrant textured surface. Consequently, the liquid will be prevented from penetrating the solid texture and producing a composite solid-liquid-vapor interface (Xu et al., 2021). Such a composite interface, corresponding to a Cassie state, appears to have high contact angles even when low-surface-tension liquids are applied (Li et al., 2019).

Besides, it is found out the order of silica nanoparticles affect the water and MDEA contact angle, which affect the superomniphobicity of the membrane. The water and MDEA contact angle exhibited by M-N2 and M-L2 are higher than M-L1 and M-N1 membranes. M-N2 shows an increment of 37.77 $^\circ$ in water contact angle and 44.50 $^\circ$ in MDEA contact angle compared to M-N1. This is due to the NH_2 functionalized silica nanoparticles is incorporated as non-solvent additives for M-N2 membrane. It shows a similar trend for M-L2 and M-L1 membranes. The water contact angle of the membrane as M-L2 is increased from $135.99 \pm 0.56^\circ$ to $164.97 \pm 2.81^\circ$ and MDEA contact angle is improved from $126.34 \pm 3.96^\circ$ to $153.3 \pm 2.13^\circ$ compared to M-L1. It is because LUDOX HS-40 silica nanoparticles are incorporated as non-solvent additives for M-L2 membrane. It can be concluded that the order of incorporation of silica nanoparticles affect the contact angle of the membrane.

This research's finding is in good agreement with the study done by Toh et al. (2020), who highlighted that the increase in contact angle measurements due to the order of nanoparticles addition was ascribed to the decrease in surface free energy and the formation of a hierarchical nano scale structure (Toh et al., 2020). Reduced surface free energy reduced the binding of liquid molecules with the membrane surface (Zhang et al., 2012). In the meantime, hierarchical surface roughness entrapped a large number of air pockets in the surface's ups and downs, reducing its contact with liquid. Due to low surface free energy and the entrainment of air, liquid molecules were unable to penetrate the valley, and as a result, their imprint was diminished. This led to an increase in membrane hydrophobicity and a decrease in the propensity for pore wetting (Kharraz et al., 2020). In addition, the inclusion of a hydrocarbon chain imposed a large resistance on the liquid phase, hence enhancing the wetting resistance of the membrane (Chiao et al., 2022).
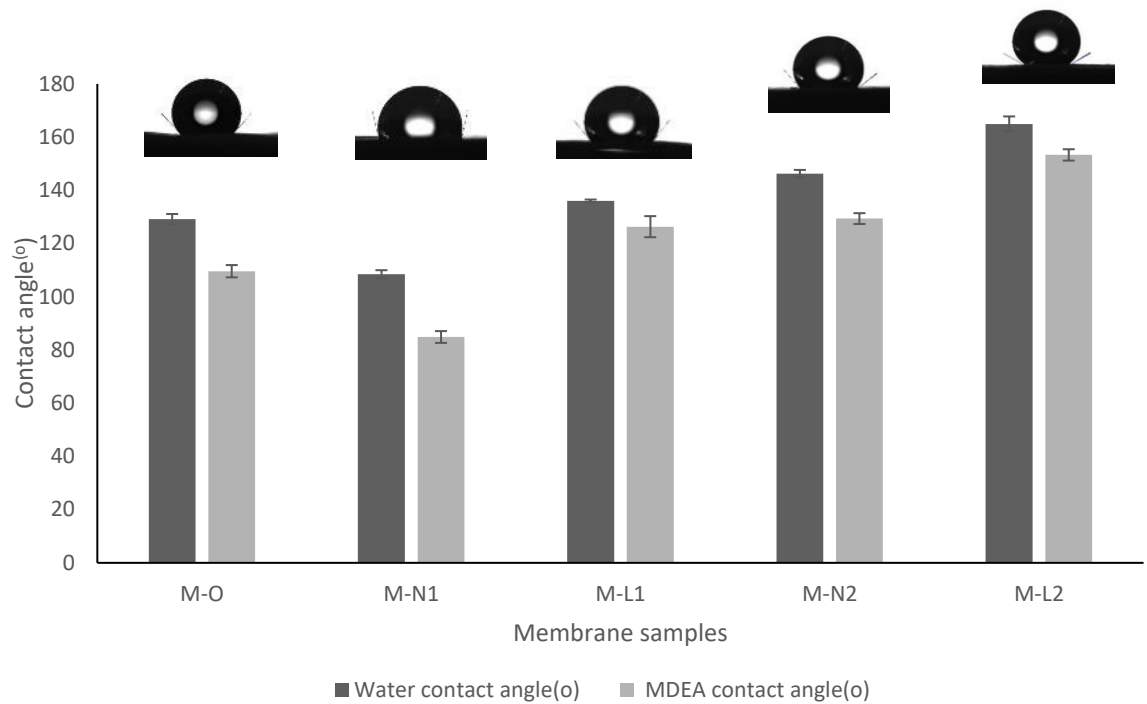
Figure 4.7: Contact angle of synthesized membranes using water and MDEA

4.3.4 Porosity Analysis

Figure 4.8 displays the results of gravimetric analysis on both the PVDF-HFP membrane and other synthesized membranes to determine their porosity. M-N2 and M-L2 exhibit higher porosity than the pristine membrane, which are $76.41 \pm 2.24\%$ and $86.24 \pm 0.95\%$ porosity, respectively. It shows an increment of 14.18 and 24.01% membrane porosity compared to M-O membrane. This result is in good agreement with the study by Tian et al. (2017), who explained the lowest porosity was found in the control substrate, which is around 60% porosity and the highest porosity with 83% was found in the silica-loaded thin film nanocomposite (TFN) polyamide FO membranes. Tian et al. concluded that with silica nanoparticle loading, the porosity of the membrane is dramatically improved (Tian et al., 2017). Another study by Zhu et al. also mentioned that the incorporation of silica nanoparticles resulted in a significant effect on membrane porosity and thickness and this can be explained by a compromise between a thermodynamic boost and a rheological hindrance (Zhu et al., 2014).

From Figure 4.8, it is observed the order of silica nanoparticles affects the porosity. The porosity of M-L2 and M-N2 membranes are higher than M-L1 and M-N1 membranes. M-N2 shows an increment of 4.73% porosity compared to M-N1. This is due to the NH_2 functionalized silica nanoparticle is incorporated as non-solvent additives for M-N2 membrane. It shows a similar trend for M-L2 and M-L1 membranes. The porosity of the membrane as M-L2 is increased from $78.39 \pm 1.22\%$ to $86.24 \pm 0.95\%$ compared to M-L1. It is because LUDOX HS-40 silica nanoparticles are incorporated as non-solvent additives for M-L2 membrane. It is concluded that the order of incorporation of silica nanoparticles affects the porosity of the membrane. This result is in agreement with the research done by Zhu et al. (2014) who study on the effect of polyvinylidene fluoride (PVDF) membrane using bio-based ginger extract-silica nanoparticles (GE-SiNPs). They mentioned that membranes show increasing porosity with the loading of GE-SiNPS as non-solvent additives (Zhu et al., 2014).

Generally, the higher membrane porosity promotes a higher gas transport across the membrane due to higher gas-liquid contact area. This statement is supported by the study of Ramezani et al. (2022) that mentioned CO_2 mass transport is substantially influenced by porosity. The effective diffusion coefficient of CO_2 inside the membrane side has a direct correlation with membrane porosity (Ramezani et al., 2022). It indicates that increasing the membrane's porosity results in a large increase in membrane diffusivity and increment in the mass transfer of CO_2 inside the membrane side. This circumstance leads to an increase in CO_2 removal efficiency under non-wetting condition. Faria et al. (2017) investigated the influence of porosity and pore size on the performance of PTFE hollow fibres, and their findings demonstrated that an increase in membrane porosity and pore size in the non-wetting zone enhanced CO_2 removal efficiency (Faria et al., 2017). The finding by Faria et al. is in agreement with this study as the highest porosity is achieved by M-L2 membrane, which results in M-L2 membrane having the highest CO_2 removal efficiency.
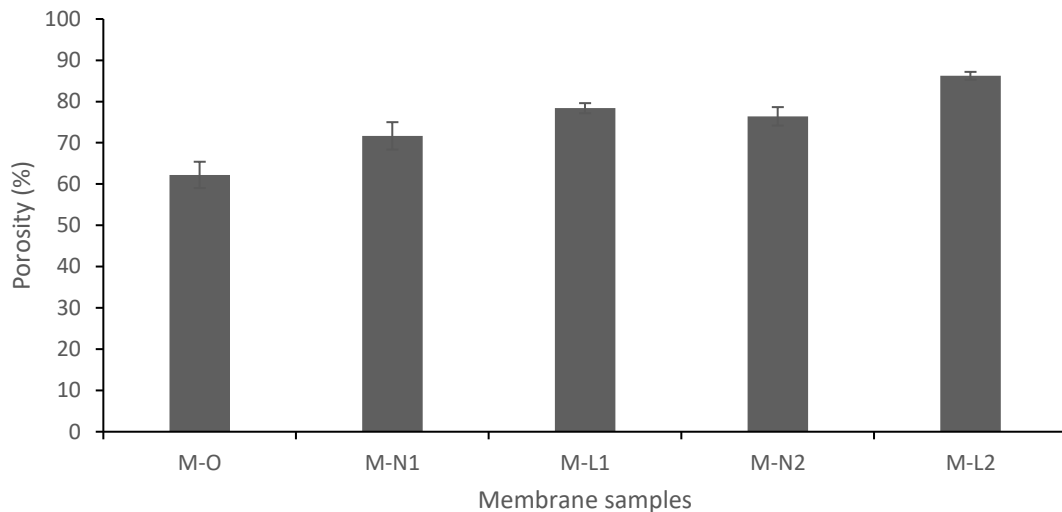
Figure 4.8: Porosity of membrane

4.4 Gas Absorption Test

Long-term immersion was used to study the deterioration of CO_2 flow that occurred due to membrane wetting. As a liquid absorbent, 1.5 molL^{-1} of MEA solution was employed to examine the performance of membranes. Figure 4.9 illustrates the influence of immersion time on CO_2 flux membrane absorption performance.

The performance of three membranes, which are M-O, M-H and M-L2 are compared over 0-day, 3-day and 6-day immersion. Prior to immersion (0-day immersion), M-O exhibits the lowest CO_2 absorption flux, which is 0.009382 mol/m^{2}s. Whereas, CO_2 absorption flux of 0.014147 mol/m^{2}s is achieved by M-H membrane. Among the three membranes, M-L2 membrane has the highest CO_2 absorption flux in MGA system, which is 0.015905 mol/m^{2}s. Despite the extensive assembly of silica nanoparticles on the surface of the PVDF-HFP membrane, they did not increase the membrane's resistance to gas transport. In comparison to pristine membranes, a comparable high CO_2 mass transfer rate is achieved by M-L2 membrane.

Research demonstrated that the silica nanoparticles loading has a slight effect on the initial absorption efficiency. According to Ying et al. (2020), the observed trend was related to the porosity feature. High porosity membranes increased the contact

area between the gas and liquid phases, hence decreasing the membrane's resistance to gas movement. The porosity analysis (see Figure 4.8) revealed that the M-L2 membrane has a porosity of 86.24% in terms of nanoparticle loading, which was greater than that of pristine membranes. This explained the observed pattern in the initial CO_2 flux.
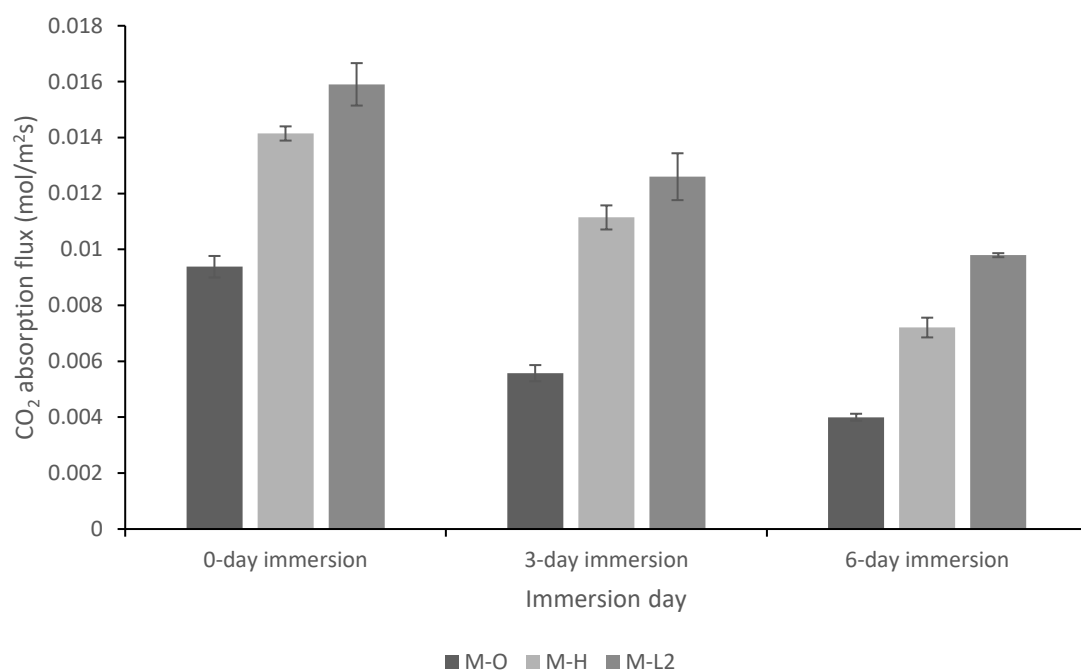
Figure 4.9: Performance of membranes over 0-day, 3-day and 6-day immersion

After immersion of 3 days, the CO_2 transfer rate of pristine membrane is dropped from 0.009382 mol/m^{2}s to 0.005575 mol/m^{2}s, which is around 40.58%. Whereas, the M-L2 has an absorption performance that dropped remarkably by 20.76%, which is from 0.015905 mol/m^{2}s to 0.012602 mol/m^{2}s as shown in Table 4.3. This is followed by M-H membrane, which shows a decrease of 22.22 % in CO_2 transfer rate. M-L2 membrane shows the lowest decrement in CO_2 absorption flux, which indicated M-L2 has the highest stability compared to M-O and M-H membranes upon 3-day immersion in 1.5 M MEA solution. In the MGA system, the M-L2 membrane exhibited a higher operational stability that was 1.95 times that of the pristine membrane. This is in a good agreement with the research done by Zargar et al. (2017) on PDMS organic solvent nanofiltration membranes using modified mesoporous silica nanoparticles. They found that integration of nanoparticle (NP) with

membranes enhanced the membranes' mechanical stability, thermal resistance, as well as their selectivity (Zargar et al., 2017).

Besides, it can be observed that the M-L2 membrane has the highest CO_2 absorption flux after immersion of 3 days. This circumstance could be explained by the study done by Cheng et al. (2018) that mentioned that high gas permeation is achieved due to its porosity. Consequently, this membrane demonstrates exceptional gas separation performance for CO_2 capture and provides an efficient strategy for fabricating high-flux membranes that are desirable for industrial applications (Cheng et al., 2018). Zou and Zhu also emphasized that high porosity is the prerequisite for high permeability (Zou & Zhu, 2018).

A significant decline in performance was observed after 6 days of immersion of the membranes in 1.5M MEA solution. The absorption efficiency of the pristine membrane decreased by 57.37 %, which is from 0.009382 mol/m^{2}s to 0.003999 mol/m^{2}s as shown in Table 4.3. The reduction in performance reached 49.05 % with 6-day immersion. Despite the fact that the M-H membrane exhibited a high MEA contact angle of 137.50°, its hydrophobicity is insufficient to guarantee a satisfactory anti-wettability. Infiltration of liquid absorbent into membrane pores still occurred, resulting in a partially wetted mode that consequently degraded CO_2 flux. The M-L2 membrane has resulted in a more stable CO_2 absorption flux in the MGA system when compared to M-O membrane as M-L2 membrane exhibits a decrease of 38.42% in CO_2 absorption flux. Due to the incorporation of silica nanoparticles, M-L2 shows the highest stability upon 6-day immersion. Similarly, the research done by Toh et al. (2020) shows the same trend as this research, who emphasized the lowest deterioration of performance for CO_2 transfer rate was exhibited by the incorporation of polydimethylsiloxane-grafted-silica (PGS) on membrane, which only declined for 8.6% in absorption flux (Toh et al., 2020).

As shown in Table 4.3, the highest CO_2 absorption flux is achieved by M-L2 membrane upon immersion of 0 days, 3 days and 6 days. This is supported by the study done by Zhu et al. (2014) on polyvinylidene fluoride (PVDF) membrane using bio-based ginger extract-silica nanoparticles (GE-SiNPs). Zhu et al. (2014) mentioned that

porosity and macro void development in membrane structure have a substantial effect on the flux performance. Other than that, Ahmad et al (2013) found that increasing the contact angle of the membrane increased CO_2 transfer rate. Due to the decrease in wetting degree by a rise in membrane hydrophobicity, the absorption flux and operational stability are improved (Ahmad et al., 2013). In the long run, mass transfer rate is more stable due to the membrane's strong hydrophobicity, which had a low affinity for liquid absorbent. Therefore, it is concluded that the incorporation of silica nanoparticles as non-solvent additives could increase the CO_2 absorption flux and operational stability of the membrane in MGA system.

Table 4.3: Performance of membranes over 0-day, 3-day and 6-day immersion at time 10, 20 and 30 minutes

Membrane samples	Time (min)	CO_2 absorption flux (mol/m^{2}s)		
		0-day	3-day	6-day
M-O	10	0.009036	0.005556	0.003879
	20	0.009314	0.005874	0.003991
	30	0.009796	0.005296	0.004127
	Average	0.009382 ± 0.0004	0.005575 ± 0.0003	0.003999 ± 0.0001
M-H	10	0.01339	0.010304	0.007132
	20	0.014908	0.01198	0.007214
	30	0.014144	0.01115	0.007276
	Average	0.014147 ± 0.0007	0.011145 ± 0.0008	0.007207 ± 0.0001
M-L2	10	0.016198	0.013067	0.009498
	20	0.015758	0.012521	0.009701
	30	0.015758	0.012217	0.010185
	Average	0.015905 ± 0.0002	0.012602 ± 0.0004	0.009795 ± 0.0003

CHAPTER 5

CONCLUSION AND RECOMMENDATIONS

5.1 Overview

This chapter provides the research study's conclusion as well as several recommendations for future work.

5.2 Conclusion

In conclusion, the first part of this study focused on the influence of silica nanoparticles and chemical additives on membrane morphology and superomniphobicity. Different silica nanoparticles and chemical additives, such as 0.06 % (wt.) LUDOX HS-40 silica nanoparticles,0.06 wt% NH_2 functionalized silica nanoparticles, 7.5 M NaOH aqueous solution, 3% v/v APTES/ethanol, 1% v/ v FAS/n-Hexane and net spacer imprinting, were utilized in order to increase the membrane superomniphobicity. By immersing in APTES/ethanol bath, M-E membrane exhibited denser top surface microstructure of compared to that of M-O membrane, the pristine membrane as slower vapour uptake rate was observed and the morphology revealed the predominance of PVDF-HFP crystal spherulites. M-H membrane with high surface roughness was obtained after immersing in FAS/n-hexane for 24 hours. It exhibited a hierarchical structure composed of polymer nodules in the morphology, which increased water and MDEA contact angles. High fluorine content, which is around 46.50 wt%, was also detected on M-H membrane. Among all, M-H membrane achieved the highest water and MDEA contact angles, which are $137.50 \pm 0.80^{\circ}$ and $133.59 \pm 1.22^{\circ}$ respectively. High surface roughness increased fluorine content and

the hierarchical structure exhibited by M-H membrane result in improvement of 6.44 and 21.89% in water and MDEA contact angles compared to the pristine membrane. However, M-L1 showed the highest porosity, which is around $78.39 \pm 1.22\%$. Despite having a greater contact angle than M-L1 membrane, M-H membrane had a lower porosity than M-L1 membrane. Compared to M-L1 membrane, the porosity of M-H membrane was reduced by 5.05% as M-H membrane displays a dense structure due to fluorination.

For further enhancement of membrane superomniphobicity, the order of silica nanoparticles addition on membrane was manipulated. 0.06 wt% LUDOX HS-40 colloidal silica nanoparticles and 0.06 wt% NH_2 functionalized silica nanoparticles were incorporated as non-solvent additive in ethanol coagulation bath. The morphology and wetting properties of membrane were investigated. Denser structure was observed in M-N2 and M-L2 membranes compared to pristine membrane. It is because the addition of hydrophobic silica nanoparticles intensified the delayed phase inversion and facilitated a greater degree of polymer crystallization during the precipitation process. Compared to M-N2 membrane, M-L2 contained higher fluorine and silicon content, which were 46.46 wt% of F content and 0.36 wt% of Si content. The increased fluorination and migration of silica nanoparticles on the membrane caused an increment in the weight percent content of F and Si contact, thus improving the contact angle and enhancing the membrane's superomniphobicity. The highest water and MDEA contact angle were achieved by M-L2 membrane, which showed $164.97^{o} \pm 2.81$ in water contact angle and $153.31^{o} \pm 2.13$ in MDEA contact angle. Besides, the highest membrane porosity was exhibited by M-L2 membrane, which indicated higher gas transport across the membrane due to higher gas-liquid contact area. Therefore, by incorporating 0.06 wt% LUDOX HS-40 colloidal silica nanoparticles as non-solvent additive in ethanol coagulation bath, M-L2 membrane achieved superomniphobicity with water and MDEA contact angles exceeding 150°. The incorporation of non-solvent additive was found to be more effective in improving membrane superomniphobicity in terms of contact angle and porosity.

To evaluate the stability on the synthesized superomniphobic membrane for the membrane gas absorption (MGA) system, long-term immersion in MEA solution was used to study the deterioration of CO_2 flow that occurred due to membrane wetting

and 1.5 $molL^{-1}$ of MEA solution was employed to examine the performance of membranes. The highest CO_2 absorption flux was achieved by M-L2 membrane as high porosity of M-L2 membrane increased the contact area between the gas and liquid phases, hence decreasing the membrane's resistance to gas movement. Upon 3-day and 6-day immersion, M-L2 membrane exhibited the highest operational stability among M-O and M-H membranes due to its higher wetting resistance. When compared to a pristine membrane, the M-L2 membrane in the MGA system showed 1.95 times greater operational stability. The result of this research indicated that addition of silica nanoparticles as a non-solvent additive to membranes could be a viable method for enhancing the anti-wettability of membranes for MGA system.

5.3   Recommendations

Prior to commercialization, the recommendation of this work is future research on hollow fibre membrane using the superomniphobic membrane should be conducted. Flat sheet configuration is used in this work for the membrane synthesized. However, hollow fibre membrane has high interfacial area, high mechanical strength and operational flexibility compared to flat sheet membrane. In addition, hollow fibre membranes can operate at high pressures, which is important for efficient CO_2 absorption. High pressure allows for a higher concentration gradient between the gas and liquid phases, resulting in a greater driving force for CO_2 absorption. Flat sheet membranes, on the other hand, are limited in their ability to operate at high pressures due to their lower strength and stability. As a result, hollow fibre membrane is frequently employed in industrial applications for gas and liquid separation.

Besides, imprinting of net spacer on the membrane should be further investigated as net spacer can improve the membrane's antifouling properties, enhance self-cleaning and reduce the adhesion of unwanted materials to the membrane surface. In addition, the analysis of the membrane surface chemistry should be conducted by using the Fourier Transform Infrared Spectroscopy. The functional groups of the PVDF-HFP membrane before and after incorporating silica nanoparticles and surface

fluorination should be examined as the change in the functional group in the membrane could affect the membrane superomniphobicity.

The stability of the nanoparticles incorporated into the polymer matrix plays a crucial role in preserving the hydrophobicity of the membrane. In MGA system, membranes are exposed to a variety of operating conditions that could detach the nanoparticles. In order to evaluate the stability of the synthesized membrane under industrial conditions, the gas absorption test could be conducted under varying temperatures, pressures and fluid velocities. The operating temperature of the membrane gas absorption process can affect the stability of the membrane. High temperatures can cause thermal degradation of the membrane material or alter its surface properties, leading to a loss of selectivity or permeability. The pressure at which the membrane is operating can also affect its stability. High-pressure differentials can cause deformation or damage to the membrane material, affecting its performance over time.

REFERENCES

Abd, A. A., Naji, S. Z., Hashim, A. S., & Othman, M. H. D. (2020). Carbon dioxide removal through physical adsorption using carbonaceous and non-carbonaceous adsorbents: A review. *Journal of Environmental Chemical Engineering*, *8*(5), 104142. https://doi.org/10.1016/j.jece.2020.104142

Abdullah, N., Rahman, M. A., Othman, M. H. D., & Ismail, A. F. (2018). Membranes and Membrane Processes. *Elsevier EBooks*, 45–70. https://doi.org/10.1016/b978-0-12-813549-5.00002-5

Ahmad, A., Mohammed, H. N., Ooi, B. S., & Leo, C. P. (2013). Deposition of a polymeric porous superhydrophobic thin layer on the surface of poly(vinylidenefluoride) hollow fiber membrane. *Polish Journal of Chemical Technology*, *15*(3), 1–6. https://doi.org/10.2478/pjct-2013-0036

Ahmad, A., & Ramli, W. K. W. (2013a). Hydrophobic PVDF membrane via two-stage soft coagulation bath system for Membrane Gas Absorption of CO2. *Separation and Purification Technology*, *103*, 230–240. https://doi.org/10.1016/j.seppur.2012.10.032

Ahmad, A., & Ramli, W. K. W. (2013b). Hydrophobic PVDF membrane via two-stage soft coagulation bath system for Membrane Gas Absorption of CO2. *Separation and Purification Technology*, *103*, 230–240. https://doi.org/10.1016/j.seppur.2012.10.032

AlMarzooqi, F., Bilad, M. R., & Arafat, H. A. (2017). Improving Liquid Entry Pressure of Polyvinylidene Fluoride (PVDF) Membranes by Exploiting the Role of Fabrication Parameters in Vapor-Induced Phase Separation VIPS and Non-Solvent-Induced Phase Separation (NIPS) Processes. *Applied Sciences*, *7*(2), 181. https://doi.org/10.3390/app7020181

Andrew Baker. (2021). *Rise in Global Natural Gas Demand*.

Arshadi, M., Taghvaei, H., Abdolmaleki, M. K., Lee, M., Eskandarloo, H., & Abbaspourrad, A. (2019). Carbon dioxide absorption in water/nanofluid by a

symmetric amine-based nanodendritic adsorbent. *Applied Energy*, *242*, 1562–1572. https://doi.org/10.1016/j.apenergy.2019.03.105

Bing-Bing, W., Hua-Ping, W., Zheng, Z., Chen-Chen, D., & Guozhong, C. (2015). Thermodynamic analysis of stable wetting states and wetting transition of micro/nanoscale structured surface. *Chinese Physics*, *64*(17), 176801. https://doi.org/10.7498/aps.64.176801

Buonomenna, M. (2017). Membrane Separation of CO2 from Natural Gas. *Recent Patents on Materials Science*, *10*(1). https://doi.org/10.2174/1874464810666170303111509

Buonomenna, M., Macchi, P., Davoli, M., & Drioli, E. (2007). Poly(vinylidene fluoride) membranes by phase inversion: the role the casting and coagulation conditions play in their morphology, crystalline structure and properties. *European Polymer Journal*, *43*(4), 1557–1572. https://doi.org/10.1016/j.eurpolymj.2006.12.033

Buzatu, P., Zsirai, T., Aerts, P., & Judd, S. J. (2012). Permeability and clogging in an immersed hollow fibre membrane bioreactor. *Journal of Membrane Science*, *421–422*, 342–348. https://doi.org/10.1016/j.memsci.2012.07.039

Cao, Z., Stevens, M. J., Carrillo, J. Y., & Dobrynin, A. V. (2015). Adhesion and Wetting of Soft Nanoparticles on Textured Surfaces: Transition between Wenzel and Cassie–Baxter States. *Langmuir*, *31*(5), 1693–1703. https://doi.org/10.1021/la5045442

Carlson, S., Becker, M., Brünig, F. N., Ataka, K., Cruz, R., Yu, L., Tang, P., Kanduč, M., Haag, R., Heberle, J., Makki, H., & Netz, R. R. (2021). Hydrophobicity of Self-Assembled Monolayers of Alkanes: Fluorination, Density, Roughness, and Lennard-Jones Cutoffs. *Langmuir*, *37*(47), 13846–13858. https://doi.org/10.1021/acs.langmuir.1c02187

Chamani, H., Woloszyn, J., Matsuura, T., Rana, D., & Lan, C. Q. (2021). Pore wetting in membrane distillation: A comprehensive review. *Progress in Materials Science*, *122*, 100843. https://doi.org/10.1016/j.pmatsci.2021.100843

Chang, P. C., Ng, Q. H., Ahmad, A. L., & Low, S. C. (2021). A critical review on the techno-economic analysis of membrane gas absorption for CO_2 capture. *Chemical Engineering Communications*, *209*(11), 1553–1569. https://doi.org/10.1080/00986445.2021.1977926

Chen, B., Zheng, X., Bai, Y., Padture, N. P., & Huang, J. (2017). Progress in Tandem Solar Cells Based on Hybrid Organic–Inorganic Perovskites. *Advanced Energy Materials*, *7*(14), 1602400. https://doi.org/10.1002/aenm.201602400

Cheng, Y., Ying, Y., Japip, S., Jiang, S., Chung, T., Zhang, S., & Zhao, D. (2018). Advanced Porous Materials in Mixed Matrix Membranes. *Advanced Materials*, *30*(47), 1802401. https://doi.org/10.1002/adma.201802401

Chiam, C., & Sarbatly, R. (2013). Vacuum membrane distillation processes for aqueous solution treatment—A review. *Chemical Engineering and Processing*, *74*, 27–54. https://doi.org/10.1016/j.cep.2013.10.002

Chiao, Y., Cao, Y., Ang, M. B. M. Y., Sengupta, A., & Wickramasinghe, S. R. (2022a). Application of superomniphobic electrospun membrane for treatment of real produced water through membrane distillation. *Desalination*, *528*, 115602. https://doi.org/10.1016/j.desal.2022.115602

Chiao, Y., Cao, Y., Ang, M. B. M. Y., Sengupta, A., & Wickramasinghe, S. R. (2022b). Application of superomniphobic electrospun membrane for treatment of real produced water through membrane distillation. *Desalination*, *528*, 115602. https://doi.org/10.1016/j.desal.2022.115602

Cui, Z., & deMontigny, D. (2013). Part 7: A review of CO_2 capture using hollow fiber membrane contactors. *Carbon Management*, *4*(1), 69–89. https://doi.org/10.4155/cmt.12.73

Darband, G. B., Aliofkhazraei, M., Khorsand, S., Sokhanvar, S., & Kaboli, A. (2020). Science and Engineering of Superhydrophobic Surfaces: Review of Corrosion Resistance, Chemical and Mechanical Stability. *Arabian Journal of Chemistry*, *13*(1), 1763–1802. https://doi.org/10.1016/j.arabjc.2018.01.013

Di, W., Wang, X., Zhou, Y., Mei, Y., Wang, W., & Cao, Y. (2022). Fluorination Increases Hydrophobicity at the Macroscopic Level but not at the Microscopic Level. *Chinese Physics Letters*, *39*(3), 038701. https://doi.org/10.1088/0256-307x/39/3/038701

Estay, H., Ortiz, M. a. R., & Romero, J. (2013). A novel process based on gas filled membrane absorption to recover cyanide in gold mining. *Hydrometallurgy*, *134–135*, 166–176. https://doi.org/10.1016/j.hydromet.2013.02.012

Fan, H., & Peng, Y. (2012). Application of PVDF membranes in desalination and comparison of the VMD and DCMD processes. *Chemical Engineering Science*, *79*, 94–102. https://doi.org/10.1016/j.ces.2012.05.052

Faria, A. V., Wang, L., Xie, M., Perreault, F., Guo, W., Ma, J., & Elimelech, M. (2017). Thin-film composite forward osmosis membranes functionalized with graphene oxide–silver nanocomposites for biofouling control. *Journal of Membrane Science*, *525*, 146–156. https://doi.org/10.1016/j.memsci.2016.10.040

Figueroa, J. a. L., & Cuenca, H. (2017). Membrane Gas Absorption Processes: Applications, Design and Perspectives. *InTech EBooks*. https://doi.org/10.5772/intechopen.72306

Geyer, F., Schönecker, C., Butt, H., & Vollmer, D. (2017). CO2 Capture: Enhancing CO2 Capture using Robust Superomniphobic Membranes (Adv. Mater. 5/2017). *Advanced Materials*, *29*(5). https://doi.org/10.1002/adma.201770035

Gopalan, J., Buthiyappan, A., & Raman, A. a. A. (2022). Insight into metal-impregnated biomass based activated carbon for enhanced carbon dioxide adsorption: A review. *Journal of Industrial and Engineering Chemistry*, *113*, 72–95. https://doi.org/10.1016/j.jiec.2022.06.026

Hamzah, N., & Leo, C. P. (2017). Membrane distillation of saline with phenolic compound using superhydrophobic PVDF membrane incorporated with TiO 2 nanoparticles: Separation, fouling and self-cleaning evaluation. *Desalination*, *418*, 79–88. https://doi.org/10.1016/j.desal.2017.05.029

Han, S., Yang, R., Li, C., & Yang, L. (2019). The Wettability and Numerical Model of Different Silicon Microstructural Surfaces. *Applied Sciences*, *9*(3), 566. https://doi.org/10.3390/app9030566

Hussin, F., & Aroua, M. K. (2020). Recent trends in the development of adsorption technologies for carbon dioxide capture: A brief literature and patent reviews (2014–2018). *Journal of Cleaner Production*, *253*, 119707. https://doi.org/10.1016/j.jclepro.2019.119707

International Energy Agency (IEA). (2022). Global short-term gas demand growth. *Oil and Gas Journal*.

Ji, D., Xiao, C., An, S., Liu, H., Chen, K., Hao, J., & Zhang, T. M. (2018). Preparation of PSF/FEP mixed matrix membrane with super hydrophobic surface for efficient water-in-oil emulsion separation. *RSC Advances*, *8*(18), 10097–10106. https://doi.org/10.1039/c8ra00055g

Jiao, L., Chua, Z. Y., Moon, S. K., Song, J., Bi, G., & Zheng, H. (2018). Femtosecond Laser Produced Hydrophobic Hierarchical Structures on Additive Manufacturing Parts. *Nanomaterials*, *8*(8), 601. https://doi.org/10.3390/nano8080601

Khan, I. A., El-Naas, M. H., Wood, D. A., & Van Der Bruggen, B. (2018). CO_2 Capture Using Hollow Fiber Membranes: A Review of Membrane Wetting. *Energy & Fuels*, *32*(2), 963–978. https://doi.org/10.1021/acs.energyfuels.7b03493

Kharraz, J. A., Farid, M. S., Khanzada, N. K., Deka, B. J., Arafat, H. A., & An, A. K. (2020). Macro-corrugated and nano-patterned hierarchically structured superomniphobic membrane for treatment of low surface tension oily wastewater by membrane distillation. *Water Research*, *174*, 115600. https://doi.org/10.1016/j.watres.2020.115600

Kim, S., Scholes, C. A., Heath, D. D., & Kentish, S. E. (2021). Gas-liquid membrane contactors for carbon dioxide separation: A review. *Chemical Engineering Journal*, *411*, 128468. https://doi.org/10.1016/j.cej.2021.128468

Kota, A. K., Kwon, G., & Tuteja, A. (2014). The design and applications of superomniphobic surfaces. *Npg Asia Materials*, *6*(7), e109. https://doi.org/10.1038/am.2014.34

Lee, E., Deka, B. J., Guo, J., Woo, Y. C., Shon, H. K., & An, A. K. (2017). Engineering the Re-Entrant Hierarchy and Surface Energy of PDMS-PVDF Membrane for Membrane Distillation Using a Facile and Benign Microsphere Coating. *Environmental Science & Technology*, *51*(17), 10117–10126. https://doi.org/10.1021/acs.est.7b01108

Lei, Y., Wang, Q., & Huo, J. (2014). Fabrication of durable superhydrophobic coatings with hierarchical structure on inorganic radome materials. *Ceramics International*, *40*(7), 10907–10914. https://doi.org/10.1016/j.ceramint.2014.03.087

Li, J., Guo, S., Xu, Z., Pan, Z., Du, Z., & Cheng, F. (2019). Preparation of omniphobic PVDF membranes with silica nanoparticles for treating coking wastewater using direct contact membrane distillation: Electrostatic adsorption vs. chemical bonding. *Journal of Membrane Science*, *574*, 349–357. https://doi.org/10.1016/j.memsci.2018.12.079

Lin, Y., Xu, Y., Loh, C. H., & Wang, R. (2018). Development of robust fluorinated TiO2/PVDF composite hollow fiber membrane for CO2 capture in gas-liquid membrane contactor. *Applied Surface Science*, *436*, 670–681. https://doi.org/10.1016/j.apsusc.2017.11.263

Liu, T. L., Chen, Z., & Kim, C. (2015). A dynamic Cassie–Baxter model. *Soft Matter*, *11*(8), 1589–1596. https://doi.org/10.1039/c4sm02651a

Liu, Y., Xiao, T., Bao, C., Fu, Y., & Yang, X. (2018). Fabrication of novel Janus membrane by nonsolvent thermally induced phase separation (NTIPS) for enhanced performance in membrane distillation. *Journal of Membrane Science*, *563*, 298–308. https://doi.org/10.1016/j.memsci.2018.05.067

Lu, K., Zuo, J., Chang, J., Kuan, H. C., & Chung, T. (2018). Omniphobic Hollow-Fiber Membranes for Vacuum Membrane Distillation. *Environmental Science & Technology*, *52*(7), 4472–4480. https://doi.org/10.1021/acs.est.8b00766

Lu, N., Jin, Y., Deng, Y., E, J., Zhao, X., Han, D., & Zhang, Z. (2018). Wetting Models and Working Mechanisms of Typical Surfaces Existing in Nature and Their Application on Superhydrophobic Surfaces: A Review. *Advanced Materials Interfaces*, *5*(1), 1701052. https://doi.org/10.1002/admi.201701052

Mokhatab, S., Poe, W. A., & Mak, J. Y. (2019). Basic Concepts of Natural Gas Processing. *Elsevier EBooks*, 177–189. https://doi.org/10.1016/b978-0-12-815817-3.00004-6

Molchanova, N., Hansen, P. R., Damborg, P., Nielsen, H. M., & Franzyk, H. (2017). Lysine-Based α-Peptide/β-Peptoid Peptidomimetics: Influence of Hydrophobicity, Fluorination, and Distribution of Cationic Charge on Antimicrobial Activity and Cytotoxicity. *ChemMedChem*, *12*(4), 312–318. https://doi.org/10.1002/cmdc.201600553

Mosadegh-Sedghi, S., Rodrigue, D., Brisson, J., & Iliuta, M. C. (2014). Wetting phenomenon in membrane contactors – Causes and prevention. *Journal of Membrane Science*, *452*, 332–353. https://doi.org/10.1016/j.memsci.2013.09.055

Norahim, N., Yaisanga, P., Faungnawakij, K., Charinpanitkul, T., & Klaysom, C. (2018). Recent Membrane Developments for CO_2 Separation and Capture. *Chemical Engineering & Technology*, *41*(2), 211–223. https://doi.org/10.1002/ceat.201700406

Odirile, P. T., Marumoloa, P. M., Manali, A., & Gikas, P. (2021). Anaerobic Digestion for Biogas Production from Municipal Sewage Sludge: A Comparative Study between Fine Mesh Sieved Primary Sludge and Sedimented Primary Sludge. *Water*, *13*(24), 3532. https://doi.org/10.3390/w13243532

Ooi, B. S., Yatim, N. S. M., Ahmad, A., & Lai, S. (2012). Preparation of polyvinylidene fluoride membrane via dual coagulation bath system and its

wettability study. *Journal of Applied Polymer Science*, *124*(S1), E225–E232. https://doi.org/10.1002/app.36269

Pratten, D., & Craig, R. G. (1989). Wettability of a hydrophilic addition silicone impression material. *Journal of Prosthetic Dentistry*, *61*(2), 197–202. https://doi.org/10.1016/0022-3913(89)90373-9

Ramezani, R., Di Felice, L., & Gallucci, F. (2022). A Review on Hollow Fiber Membrane Contactors for Carbon Capture: Recent Advances and Future Challenges. *Processes*, *10*(10), 2103. https://doi.org/10.3390/pr10102103

Rana, D., Baghbanzadeh, M., Rana, D., Matsuura, T., & Lan, C. Q. (2015). Effects of superhydrophobic SiO2 nanoparticles on the performance of PVDF flat sheet membranes for vacuum membrane distillation. *Desalination*, *373*, 47–57. https://doi.org/10.1016/j.desal.2015.07.002

Rosnan, N. '., Haan, T. Y., & Mohammad, A. W. (2018). The Effect of ZnO Loading for the Enhancement of Psf/ZnO-GO Mixed Matrix Membrane Performance. *Sains Malaysiana*, *47*(9), 2035–2045. https://doi.org/10.17576/jsm-2018-4709-11

Ryu, J. K., Messersmith, P. B., & Lee, H. (2018). Polydopamine Surface Chemistry: A Decade of Discovery. *ACS Applied Materials & Interfaces*, *10*(9), 7523–7540. https://doi.org/10.1021/acsami.7b19865

Sabzekar, M., Chenar, M. P., Khayet, M., García-Payo, C., Maghsoud, Z., & Pagliero, M. (2022). Cyclic olefin polymer membrane as an emerging material for CO2 capture in gas-liquid membrane contactor. *Journal of Environmental Chemical Engineering*, *10*(3), 107669. https://doi.org/10.1016/j.jece.2022.107669

Shawky, A., Noor, M. J. M. M., Nasef, M. M., Khayet, M., Nallappan, M. L., & Ujang, Z. (2016). Enhancing antimicrobial properties of poly(vinylidene fluoride)/hexafluoropropylene copolymer membrane by electron beam induced grafting of N-vinyl-2-pyrrolidone and iodine immobilization. *RSC Advances*, *6*(48), 42461–42473. https://doi.org/10.1039/c5ra28091e

Tian, D., Kitamura, Y., & Li, S. (2012). Evaluation of Stirling cooler system for cryogenic CO2 capture. *Applied Energy*, *98*, 491–501. https://doi.org/10.1016/j.apenergy.2012.04.013

Tian, M., Wang, Y., Wang, R., & Fane, A. G. (2017). Synthesis and characterization of thin film nanocomposite forward osmosis membranes supported by silica nanoparticle incorporated nanofibrous substrate. *Desalination*, *401*, 142–150. https://doi.org/10.1016/j.desal.2016.04.003

Toh, M. Y., Oh, P. C., Ahmad, A. L., & Caille, J. (2019). Enhancing membrane wetting resistance through superhydrophobic modification by polydimethylsilane-grafted-SiO2 nanoparticles. *Korean Journal of Chemical Engineering*, *36*(11), 1854–1858. https://doi.org/10.1007/s11814-019-0362-3

Toh, M. Y., Oh, P. C., Chew, T. L., & Ahmad, A. L. (2020). Preparation of polydimethylsiloxane-SiO2/PVDF-HFP mixed matrix membrane of enhanced wetting resistance for membrane gas absorption. *Separation and Purification Technology*, *244*, 116543. https://doi.org/10.1016/j.seppur.2020.116543

Wang, Y., & Gong, X. (2017). Special oleophobic and hydrophilic surfaces: approaches, mechanisms, and applications. *Journal of Materials Chemistry. A, Materials for Energy and Sustainability*, *5*(8), 3759–3773. https://doi.org/10.1039/c6ta10474f

Wang, Y., Ma, Z., Zhang, X., Li, J., Zhou, Y., Jin, Z., & Li, N. (2022). Mixed-matrix membranes consisting of Pebax and novel nitrogen-doped porous carbons for CO2 separation. *Journal of Membrane Science*, *644*, 120182. https://doi.org/10.1016/j.memsci.2021.120182

Wood, D. A., Cai, J., Chen, F., Li, H., Zhang, W., & Qi, W. (2018). Progress in enhancement of CO2 absorption by nanofluids: A mini review of mechanisms and current status. *Renewable Energy*, *118*, 527–535. https://doi.org/10.1016/j.renene.2017.11.031

Wu, H., Zhu, K., Wu, B., Lou, J., Zhang, Z. G., & Chai, G. (2016). Influence of structured sidewalls on the wetting states and superhydrophobic stability of

surfaces with dual-scale roughness. *Applied Surface Science*, *382*, 111–120. https://doi.org/10.1016/j.apsusc.2016.04.101

Wu, X., Zhao, B., Wang, L., Zhang, Z., Li, J., He, X., Zhang, H., Zhao, X., & Wang, H. (2018). Superhydrophobic PVDF membrane induced by hydrophobic SiO 2 nanoparticles and its use for CO 2 absorption. *Separation and Purification Technology*, *190*, 108–116. https://doi.org/10.1016/j.seppur.2017.07.076

Xiao, Z., Guo, H., He, H., Liu, Y., Li, X., Zhang, Y., Yin, H., Volkov, A., & Chen, Y. (2020). Unprecedented scaling/fouling resistance of omniphobic polyvinylidene fluoride membrane with silica nanoparticle coated micropillars in direct contact membrane distillation. *Journal of Membrane Science*, *599*, 117819. https://doi.org/10.1016/j.memsci.2020.117819

Xu, G., Liang, F., Yang, Y., Hu, Y., Zhang, K., & Liu, W. (2014). An Improved CO2 Separation and Purification System Based on Cryogenic Separation and Distillation Theory. *Energies*, *7*(5), 3484–3502. https://doi.org/10.3390/en7053484

Xu, Y., Yang, Y., Fan, X., Liu, Z., Li, D., Wang, Y., Tao, P., Song, C., & Shao, M. (2021). In-situ silica nanoparticle assembly technique to develop an omniphobic membrane for durable membrane distillation. *Desalination*, *499*, 114832. https://doi.org/10.1016/j.desal.2020.114832

Yao, C., Garvin, T. P., Alvarado, J. L., Jacobi, A. M., Jones, B. G., & Marsh, C. P. (2012). Droplet contact angle behavior on a hybrid surface with hydrophobic and hydrophilic properties. *Applied Physics Letters*, *101*(11), 111605. https://doi.org/10.1063/1.4752470

Ying, Y., Tong, M., Ning, S., Ravi, S. K., Peh, S. B., Tan, S. T., Pennycook, S. J., & Zhao, D. (2020). Ultrathin Two-Dimensional Membranes Assembled by Ionic Covalent Organic Nanosheets with Reduced Apertures for Gas Separation. *Journal of the American Chemical Society*, *142*(9), 4472–4480. https://doi.org/10.1021/jacs.9b13825

Zargar, M., Hartanto, Y., Jin, B., & Dai, S. (2017). Understanding functionalized silica nanoparticles incorporation in thin film composite membranes: Interactions and desalination performance. *Journal of Membrane Science*, *521*, 53–64. https://doi.org/10.1016/j.memsci.2016.08.069

Zhang, N., Yang, N., Chen, H., Jiang, B., Sun, Y., Ma, J., Cheng, K., & Peng, F. (2020). Facile hydrophilic modification of PVDF membrane with Ag/EGCG decorated micro/nanostructural surface for efficient oil-in-water emulsion separation. *Chemical Engineering Journal*, *402*, 126200. https://doi.org/10.1016/j.cej.2020.126200

Zhang, Y., Wang, R., Zhang, L., & Fane, A. G. (2012). Novel single-step hydrophobic modification of polymeric hollow fiber membranes containing imide groups: Its potential for membrane contactor application. *Separation and Purification Technology*, *101*, 76–84. https://doi.org/10.1016/j.seppur.2012.09.009

Zhang, Y., Zhou, W., Liu, S., & Wang, R. (2013). Current status and development of membranes for CO2/CH4 separation: A review. *International Journal of Greenhouse Gas Control*, *12*, 84–107. https://doi.org/10.1016/j.ijggc.2012.10.009

Zhang, Z. P., Yan, Y. F., & Zhang, I. (2014). Hollow fiber membrane contactor absorption of CO2 from the flue gas: Review and perspective. *Global Nest Journal*, *16*(2), 354–373. https://doi.org/10.30955/gnj.001343

Zhao, S., Feron, P., Knuutila, H. K., Favre, E., Chabanon, E., Yan, S., Hou, J., Chen, V., & Qi, H. (2016). Status and progress of membrane contactors in post-combustion carbon capture: A state-of-the-art review of new developments. *Journal of Membrane Science*, *511*, 180–206. https://doi.org/10.1016/j.memsci.2016.03.051

Zhu, L., Zeng, H., Jiang, J., Yi, Z., Zhao, Y., Zhu, B., & Xu, Y. (2014). Hydrophilic and anti-fouling polyethersulfone ultrafiltration membranes with poly(2-hydroxyethyl methacrylate) grafted silica nanoparticles as additive. *Journal of Membrane Science*, *451*, 157–168. https://doi.org/10.1016/j.memsci.2013.09.053

Zou, X., & Zhu, G. (2018). Microporous Organic Materials for Membrane-Based Gas Separation. *Advanced Materials*, *30*(3), 1700750. https://doi.org/10.1002/adma.201700750

APPENDICES

APPENDIX A: Experimental Data for Contact Angles of Membranes using Water and MDEA

Table A.1: Contact angles of membranes using water and MDEA

Membrane samples	Water contact angle($^{\circ}$)	MDEA contact angle($^{\circ}$)
M-O	129.18 ± 1.92	109.60 ± 2.31
M-NaOH	39.93 ± 3.87	23.54 ± 3.03
M-S	64.77 ± 3.83	41.84 ± 0.54
M-N1	108.49 ± 1.50	84.88 ± 2.22
M-E	117.61 ± 2.83	74.83 ± 0.37
M-L1	135.99 ± 0.56	126.34 ± 3.96
M-H	137.50 ± 0.80	133.59 ± 1.22
M-N2	146.26 ± 1.42	129.38 ± 2.03
M-L2	164.97 ± 2.81	153.31 ± 2.13

APPENDIX B: Calculation of Membrane Porosity

Membrane porosity is calculated via gravimetric approach with the following equation:

$$\varepsilon = \frac{(m_1 - m_2)/\rho_P}{(m_1 - m_2)/\rho_P + m_2/\rho_m} \text{x } 100\%,$$

where m_1 represents wet weight

m_2 represents dry weight

ρ_m represents density of PVDF-HFP membrane

ρ_P represents density of Isopropanol

Table B.1: Density of membrane and isopropanol

Materials	Density (g/ml)
PVDF-HFP membrane	1.780
Isopropanol	0.785

Example: Porosity of pristine PVDF-HFP membrane (M-E). The dry and wet weight of membrane are 0.032 g and 0.056 g, respectively.

$$\varepsilon = \frac{(m_1 - m_2)/\rho_P}{(m_1 - m_2)/\rho_P + m_2/\rho_m} \text{x } 100\%$$

$$\varepsilon = \frac{(0.056 - 0.032)/0.785}{(0.056 - 0.032)/0.785 + 0.032/1.78} \text{ x } 100\%$$

$$\varepsilon = 62.97\%$$

Table B.2: Porosity of membrane

Membrane	Run	Dry Weight (g)	Wet Weight (g)	Porosity (%)
M-O	1	0.032	0.056	62.97
	2	0.043	0.07	58.74
	3	0.033	0.06	64.98
	Average			62.23 ± 3.18
M-NaOH	1	0.013	0.028	72.35
	2	0.015	0.031	70.75
	3	0.026	0.05	67.67
	Average			70.26 ± 2.38
M-S	1	0.023	0.046	69.40
	2	0.029	0.057	68.65
	3	0.037	0.071	67.57
	Average			68.54 ± 0.92

M-N1	1	0.015	0.035	75.15
	2	0.03	0.063	71.38
	3	0.025	0.049	68.52
Average				71.68 ± 3.32
M-E	1	0.027	0.062	74.62
	2	0.023	0.051	73.41
	3	0.031	0.071	74.53
Average				74.18 ± 0.67
M-L1	1	0.021	0.052	77.00
	2	0.017	0.045	78.88
	3	0.016	0.043	79.28
Average				78.39 ± 1.22
M-H	1	0.027	0.062	74.62
	2	0.023	0.052	74.09
	3	0.031	0.065	71.32
Average				73.34 ± 1.77
M-N2	1	0.016	0.039	76.52
	2	0.019	0.043	74.12
	3	0.021	0.055	78.59
Average				76.41 ± 2.24
M-L2	1	0.025	0.096	86.56
	2	0.019	0.075	86.98
	3	0.015	0.053	85.17
Average				86.24 ± 0.95

APPENDIX C: Calculation of CO_2 Absorption Flux

The CO_2 absorption flux is calculated with the following equation:

$$J = \frac{(Ql,in- Ql,out)\times\rho_g}{M_g A}$$

Example: CO_2 absorption of pristine PVDF-HFP membrane (M-O) at ambient condition with an effective area, A of 9.62×10^{-4} m^2. The gas flow rate of CO_2 inlet and outlet are 149.7896 ml/min and 138.0776 ml/min, respectively.

$$J = \frac{(149.7896 \text{ ml/min} - 138.0776 \text{ ml/min}) \times 0.00198 \ g/ml}{44.01 \ g/mol \ x \ 9.62 \ x \ 10^{-4} m^2} x \frac{1 \ min}{60 \ s}$$

$J = 0.009155$ mol/m^{2}s

Table C.1: CO_2 absorption flux of synthesize membranes for 0-day immersion, 3-day immersion and 6-day immersion

Membrane	Run	CO_2 inlet flow rate (ml/min)	CO_2 outlet flow rate (ml/min)	CO_2 absorption flux (mol/m^{2}s)
0-day immersion				
M-O	1	149.7896	138.0776	0.009155
	2	150.0763	137.6587	0.009609
	Average			0.009382
M-H	1	150.9866	133.9777	0.013249
	2	151.0633	131.5369	0.015047
	Average			0.014148
M-L2	1	150.6809	131.0562	0.015159
	2	151.4500	130.2686	0.016650
	Average			0.015905
Membrane	Run	CO_2 inlet flow rate (ml/min)	CO_2 outlet flow rate (ml/min)	CO_2 absorption flux (mol/m^{2}s)
3-day immersion				

Membrane	Run			
M-O	1	152.9138	145.4706	0.005727
	2	151.9813	144.9866	0.005423
		Average		0.005575
M-H	1	150.0786	136.2132	0.010628
	2	150.3026	134.9768	0.011661
		Average		0.011145
M-L2	1	150.5362	133.0472	0.01424
	2	149.0638	135.3743	0.010964
		Average		0.012602

Membrane	Run	CO_2 inlet flow rate (ml/min)	CO_2 outlet flow rate (ml/min)	CO_2 absorption flux (mol/m^{2}s)
		6-day immersion		
M-O	1	150.7595	145.9445	0.003789
	2	150.7595	145.3119	0.004208
		Average		0.003999
M-H	1	150.2278	138.7432	0.008913
	2	150.3778	143.2091	0.005501
		Average		0.007207
M-L2	1	150.0793	136.3626	0.010848
	2	149.9301	138.7509	0.008742
		Average		0.009795